NTNU – Trondheim
Norwegian University of
Science and Technology

Carbon-Supported Nanostructured Core-Shell Catalysts for Low Temperature Fuel Cells

Mats Jensen

Materials Science and Engineering
Submission date: June 2015
Supervisor: Svein Sunde, IMTE
Co-supervisor: Jørgen Svendby, IMTE

Norwegian University of Science and Technology
Department of Materials Science and Engineering

Prefrace

This work was written during the spring semester 2015, as a part of the course TMT4905, and is the final part of a master's degree at the Department of Materials Science and Engineering at the Norwegian University of Science and Technology (NTNU).

I want to thank my supervisors Prof. Svein Sunde and PhD Candidate Jørgen Svendby for their guidance in this project, both for the experiments and theory, and Staff Engineer Magnus Bentzen Følstad for facilitating the experimental work.

Abstract

The direct methanol fuel cell needs a catalyst with low overpotential and high current density for methanol oxidation to be commerically viable. The catalyst with highest performance at the moment is the PtRu-alloy catalyst, but this is unstable. A compromise is the core-shell catalyst with ruthenium core and platinum shell. This catalyst shows improvement for CO-oxidation, but for the overall methanol oxidation, this is not as high as expected. This is believed to be because the catalyst promotes the parallell pathway through the intermediary species formaldehyde and formic acid.

A method to detect these species were investigated. A model was made to calculate the concentration on the ring electrode to see if this was feasible. A rotating ring-disk electrode setup with a gold ring electrode was used to try and detect these species on the ring when they were formed on the disk. Experiments for different concentrations for formic acid and formaldehyde showed that palladium was more sensitive for these species than gold. An attempt to make a palladium ring by electrodeposition was made, and a microcell was also used to try and detect formaldehyde and formic acid by getting a high enough concentration in the bulk after methanol oxidation.

The conclution of these experiments were that the ring-disk experiment on gold was inconclusive, but the model and results from concentration experiments showed that it should be feasible. Most of the electrodeposited palladium electrodes were shown to be active in methanol, and the microcell experiment was inconclusive.

Sammendrag

Den direkte metanolbrensecellen trenger en katalysator med lavt overpotensiale og høy strømtetthet for metanoloksidasjon for å være kommersielt levedyktig. Katalysatoren med høyest ytelse for øyeblikket er en katalysator av PtRu-legering, men denne er ustabil. Et kompromiss er å lage en kjerne-skall-katalysator med en ruthenium kjerne og et platina skall. Denne katalysatoren viser en forbedring for CO-oksidasjon, men er ikke like god som forventet for den overordnede metanoloksidasjonen. De mener at dette er fordi katalysatoren promoterer den parallelle reaksjonsveien gjennom de foreløpige spesiene formaldehyd og maursyre.

En metode for å detektere disse spesiene ble undersøkt. En modell for å regne ut konsentrasjonen av disse på ring-elektroden ble laget for å se om dette var gjennomførbart. Et roterende ring-disk-elektrode oppsett med en gulldisk-elektrode ble brukt for å forsøke å detektere disse spesiene på ringen etter at de ble dannet på disken. Eksperimenter ved forskjellige konsentrasjoner for maursyre og formaldehyd viste at palladium var mer sensitivt for disse spesiene enn gull. Et forsøk ble gjort på å lage en palladium ring-elektrode, og en mikrocelle ble brukt for å forsøke å detektere formaldehyd og maursyre ved å få en høy nok konsentrasjon i bulken etter metanoloksidasjon.

Konklusjonen av disse eksperimentene var at ring-disk-eksperimentet på gull var resultatløst, men modellen og resultatene fra konsentrasjonseksperimentene viste at det var gjennomførbart. De fleste av de elektrodeponerte palladiumelektrodene viste seg å være aktive i metanol, og mikrocelleeksperimentet var også resultatløst.

Innhold

1. Introduction

1.1 Background

Fossil fuels are the backbone of our current energy economy, both for large scale and small scale applications [1]. Alternatives for these fuels have been sought for many years because of the well known problems involved. Problems like production for carbon dioxide when consumed, which contributes to global warming and climate changes. Air pollution is also a problem with these fuels from emissions of nitrogen oxides and sulphur dioxides. There is also the problem of production where oil is going to reach its peak production in the near future. Although oil is the most important fossil fuel, gas and coal can probably replace it for large scale applications, but that would not solve the environmental problems. For other applications, like cars, gas and coal are unsuitable as replacements, and alternative energy sources and carriers are needed.

For large scale applications, like primary energy production, the alternatives for fossil fuels are renewable sources like hydroelectric power, solar energy, geothermal energy and tidal power, but most of these have a problem with consistent energy production, and have to be used together with either other power sources, are methods to store their energy. One way to solve this is to use pumped hydropower storage which uses excess energy to pump water back up into a dam. Another way is the use the energy to produce fuels like hydrogen that can be used in fuel cells to balance the load from the renewable sources.

For vehichles, the most used alternative to fossil fuels is the electric car, but these still have several problems. The batteries have long charging times, and not good enough range for all purposes, so these are most suited for short trips and frequent

possibilities for charging. Fuel cells can be an alternative here aswell where they are used to produce electricity directly to the engine.

1.2 Fuel Cells

A fuel cell is a device that directly converts the energy of a chemical reaction into electrical energy. In comparison, an internal combustion engine converts the chemical energy to heat, which is used to generate mechanical energy. In a fuel cell, each half-reaction reacts on a different electrode seperated by an electrode with no electron conductivity. The electrons are guided through an external curcuit between the electrodes where they generate electrical work. The most well known fuel cell is the proton exchange membrane fuel cell (PEMFC). This fuel cell uses hydrogen as fuel and the only byproduct is water. On the anode, the hydrogen is oxidised on the following reaction:

$$2\mathrm{H}_2 \rightarrow 4\mathrm{H}^+ + 4\mathrm{e}^-, \qquad E^0 = 0V_{RHE} \tag{1.1}$$

and on the cathode, the oxygen is reduced:

$$O_2 + 4H^+ + 4e^- \rightarrow 2H_2O, \qquad E^0 = 1.23V_{RHE} \tag{1.2}$$

There are several different types of fuel cells that uses different types of fuels, materials or operating conditions. All of these have their own advantages and disadvantages. The solid oxide fuel cell (SOFC) is a high temperature fuel cell that uses hydrogen as a fuel and a solid oxide as its ion-carrier. This fuel cell is mostly used for a high, constant output because it has a long startup time and difficulties with adjusting the output. The main advantage that makes up for these problems is the high efficiency. The PEMFC on the other hand has a low startup time, low temperature and can easily regulate its output, but its not as efficient as the SOFC. The advantages are important for vehicles since the fuel cell have to be small and mobile, and output as much power as the vehicle need at that moment. One of the main disadvantages for these vehicles are the need to use and transport the hydrogen. In its gaseous state, the hydrogen have a very low volumetric density. This can be improved by storing the hydrogen as a liquid, but this introduces more efficiency loss from converting the hydrogen between gas and liquid. There is also safety issues concerning hydrogen since its flammable and explosive gas that has to be dealt with. On the enviorenmental side, hydrogen is mainly produced from natural gas, so the dependancy on

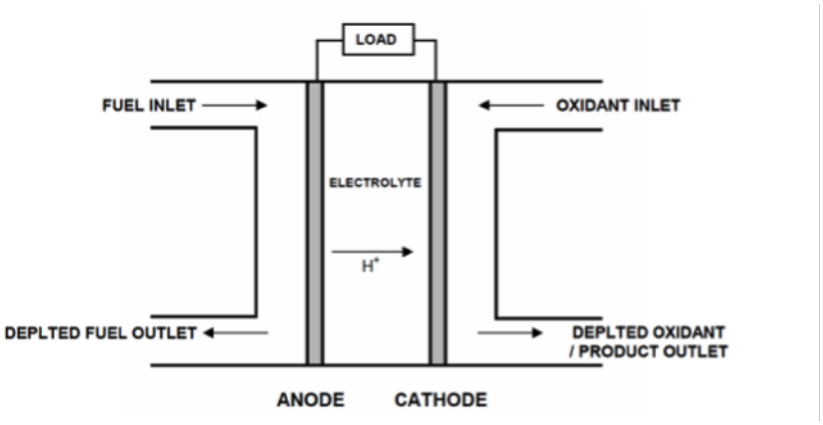

Figur 1.1: Schematic representation of a PEMFC. Taken from [3]

fossil fuels would still be an issue [2]. The solution to many of these issues is to use a fuel that is liquid at standard conditions, have a comparable energy density that can be extracted in a fuel cell, and is easy to produce. Such fuels exists in the form of for example methanol, ethanol and formic acid, altough methanol and formic acid is also mainly produced from syngas from natural gas. Methanol is our focus for this paper with the direct methanol fuel cell (DMFC).

The DMFC is similar to the PEMFC considering the principles and advantages, as it is also using a proton exchange membrane. The reaction uses methanol as fuel and the byproducts are water and carbon dioxide. The anode reaction is:

$$\mathrm{CH_3OH} + H_2O \rightarrow CO_2 + 6H^+ + 6e^- \qquad E_0 = 0.029V_{RHE} \tag{1.3}$$

and the cathode reactions is:

$$\frac{3}{2}O_2 + 6H^+ + 6e^- \rightarrow 3H_2O \qquad E_0 = 1.229V_{RHE} \tag{1.4}$$

This is a more complex reaction than the hydrogen reaction for PEM (1.1) and (1.2), and will be discussed more in a later section. The DMFC still has some issues to be improved. The membrane is conducting some methanol in addition to the protons, so that the cathode chamber gets contaminated. The main problem is the high overpotential for both the anode and cathode reactions. This can be improved by better electrocatalysts. The best catalyst at the moment is the platinum-ruthenium alloy, but this has been shown to be unstable. A compromise has been the ruthenium-platinum core-shell catalyst with a ruthenium core and a platinum shell. This catalyst has been investigated and has shown improvement over the Pt-catalyst in some

areas, but not improved others as much as expected. One theory is that the catalyst promotes the parallell pathway for methanol oxidation, which produces the intermediary species formaldehyde and formic acid. The goal of this paper is to develop a method to detect these species, and see if there is a difference between the catalysts.

2. Theory

2.1 Electrochemical methods

2.1.1 Cyclic voltammetry

Cyclic voltammetry (CV) is a common technique in electrochemical experiments. It utilizes a potential sweep to evaluate the electrochemical reaction. The potentials sweep is performed by imposing a triangular waveform as th potential on the working electrode while simultaniously recording the current on the electrode as a function of the potential. The different parameters in this method are the negative and positive turn-potentials, the start potential and direction, and the sweep rate. The triangular waveform with parameters are illustrated in figure 2.1. The voltammetry is usually performed with potentials between the hydrogen and oxygen evolution reactions, so that these wont dominate the current.

The main principle behind CV is that the current is determined by the coupling of the diffusion to the electrode and the electron transfer process on the electrode surface. The the potential for the electron transfer process is reached, the species on the electron surface will be spent and the concentration will decrease. This generates a increasing concentration gradient which increases the flux to the surface. When the surface concentration reaches zero, the gradient will decrease and the diffusion layer will increase. The current is proportional to the concentration gradient and will increase and decrease accordingly and create the characteristic peaks of CV. Increasing sweep rates will increase the concentration gradient and we get higher peaks. If there is a slow electron transfer, the potential of the peak will shift with increasing sweep rates. The processes govern the shapes of the CV. An example is

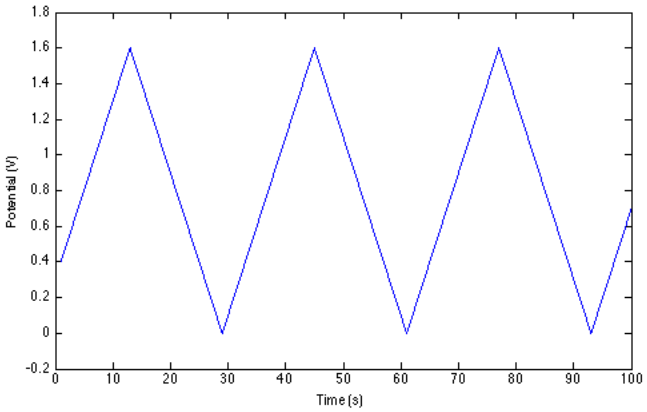

Figur 2.1: Illustration of a waveform for CV. Start potential: 0.4 V, positive turn potential: 1.6 V, negative turn potential 0 V, sweep rate: 100 mV/s and up direction.

shown in figure 2.4, which shows CO-stripping at different catalysts [4]

2.1.2 CO-stripping

CO-stripping is a technique that utilizes the same potential sweep as CV. It is performed by bubbling CO-gas through a solution and applying a potential on the working electrode where the CO will preferably adsorb on the electrode surface creating a monolayer that covers the entire surface. Afterwards argon or nitrogen is bubbled through the solution to eliminate the remaining CO in the solution. Then the potential sweep is applied where the current is measured until the CO-layer is oxidized which represents a peak in the CV. The position and shape of the peak can show us information on how the CO is oxidized on a particular electron surface or catalyst. The charge associated with oxidizing the CO can be used to calculate the active surface area of the electrode.

2.1.3 Rotating ring-disk electrode

The rotating ring-disk electrode (RRDE) is an expansion on the rotating disk electrode (RDE). The RDE consists of a disk electrode encased in teflon, while the RRDE has an additional ring electrode outside the disk insulated from the disk with te-

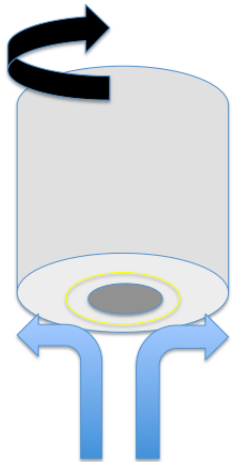

Figur 2.2: Illustration of a ring-disk electrode with rotation and flow pattern.

flon. When these electrodes are rotating they create a forced convection where the solution is drawn up along the center axis and flung out radially from them. This forced convection creates a predictable and constant diffusion layer on the surface of the electrode. This can be used to determine electrochemical characteristisk of a reaction, e.g. if the reaction is mass transport limited. Higher rotation should result in smaller diffusion layer, therefore higher concentration gradient and current.

The additional uses of RRDE compared to RDE comes from the flow pattern where products from the disk is flowing over the ring electrode. This can be used to detect products from the disk on the ring by continuing the reaction or reverse it. With a bipotansiostat, the potential on these electrodes can be controlled independently and used in different modes for different goals with the experiments. E.g. constant potential on the disk and CV on the ring, or the other way around.

2.2 Methanol oxidation

The methanol oxidation reaction (MOR) has been a popular subject of study for many years in the hope of making the DMFC commercially viable, which as yet to happen. The complete methanol to CO2 reaction is:

$$\mathrm{CH_3OH} + H_2O \rightarrow CO_2 + 6H^+ + 6e^- \qquad E_0 = 0.029V_{RHE} \tag{2.1}$$

We see that the standard equilibrium potential is close to the potential for hydrogen evolution, but the kinetics of MOR is much slower, and to get a sufficiently large current, overpotential of several hundred millivolts are necesseary [5]. The MOR can be simplified by the following parallell reactions:

$$\mathrm{CH_3OH} \rightarrow \text{adsorbed intermediaries} \begin{cases} \rightarrow \mathrm{CO_{ad}} \rightarrow \mathrm{CO_2} \\ \rightarrow \mathrm{HCHO, HCOOH} \rightarrow \mathrm{CO_2} \end{cases} \tag{2.2}$$

Where the reaction through CO is called the serial pathway and through formaldehyde and formic acid is called the parallell pathway. Formaldehyde and formic acid can be considered both intermediaries or by-products for this reaction, and formic acid has its own dual pathway oxidation. Both of these species can also form adsorbed CO when oxidized. It has been suggested that these species form from the adsorbed intermediaries $\mathrm{CH_2OH}$ and CHOH.

Platinum is the most used catalyst for MOR and a reaction mechanic on platinum has been suggested to be [5]:

$$\mathrm{CH_3OH} \longrightarrow {}_{\mathrm{x}}\mathrm{CH_2OH} + \mathrm{H^+} + \mathrm{e^-} \tag{2.3}$$
$${}_{\mathrm{x}}\mathrm{CH_2OH} \longrightarrow {}_{\mathrm{xx}}\mathrm{CHOH} + \mathrm{H^+} + \mathrm{e^-} \tag{2.4}$$
$${}_{\mathrm{xx}}\mathrm{CHOH} \longrightarrow {}_{\mathrm{xxx}}\mathrm{COH} + \mathrm{H^+} + \mathrm{e^-} \tag{2.5}$$
$${}_{\mathrm{xxx}}\mathrm{COH} \longrightarrow {}_{\mathrm{x}}\mathrm{CO} + \mathrm{H^+} + \mathrm{e^-} \tag{2.6}$$

where x stands for a Pt-site. Methanol have to adsorb on the Pt-surface, before this reaction can proceed. At low potentials, all sites are already occupied by hydrogen atoms, and methanol cannot displace these. That means that the hydrogen have to desorb before methanol can adsorb. This happens near 0.2 V vs RHE. When this has occured, we see that the methanol reaction ends in adsorbed CO, which is also a complex reaction.

For CO oxidation to $\mathrm{CO_2}$ to occur, CO has to react with some oxygen containing species, normally water. A mechanism for this has been proposed as:

$$\mathrm{H_2O} + \mathrm{s} \longleftrightarrow \mathrm{OH_{ad}} + \mathrm{H^+} + \mathrm{e^-} \tag{2.7}$$
$$\mathrm{CO_{ad}} + \mathrm{OH_{ad}} \longrightarrow \mathrm{CO_2} + \mathrm{H^+} + \mathrm{e^-} \tag{2.8}$$

where s is a Pt-site. We can see that for this reaction to proceed, water has to disassociate to hydroxide and hydrogen. On a pure platinum surface, this only happens at potentials above 0.4 - 0.45 V vs RHE. Because of this, reaction (2.8) cannot begin below 0.45 V and does not have a good reactivity below at least 0.7 V vs RHE [5]. With more advanced catalysts, this can be improved.

2.3 Catalyst for methanol oxidation reaction

The most reactive catalyst for MOR is, at the moment, a ruthenium-platinum alloy. When these elements are alloyed, we get two different effects which increases the activity of the catalyst. The first effect is the bifunctional mechanism. On ruthenium, the disassociation of water to hydroxide and hydrogen (2.7) can happen at lower potential. Then we have the same reactions as (2.7) and (2.8), only the hydroxide is adsorbed on ruthenium, and not on platinum.

The other effect is the ligand effect. This effect is associated with the electronic structure of the ruthenium atom. When an atom is placed in a lattice with atoms of a different size, or an overlayer of atoms is placed on a structure of a different material, we have a lattice mismatch. This will introduce a strain on the which leads to an inrease in the coupling between the d-bands of the atoms. This change in the d-band leads to a decrease in the bonding energy between Pt- and CO-atom [6]. This effect is comparatively small on the PtRu catalyst compared to the bifunctional mechanism.

The main problem for the PtRu catalyst is its instability. In chronoamperemetry experiments in methanol, the current does not reach a stable behaviour even after several hours. The cause of this is oxide formation of ruthenium, which is inactive for methanol. There is also dissolution of the oxide in the solution, which leads to loss of active material [7]. Another factor in this bevaiour is the apparent blocking of sites by organic species which can only be oxidized at high anodic potentials [5].

This instability can be prevented by using a core-shell catalyst. The Ru@Pt core-shell catalyst consists of a ruthenium core and a thin platinum shell (figure 2.3). We lose the bifunctional effect with this structure since there are no available ruthenium atoms for H_2O to disassociate on. The shell is thin enough that the ligand effect will remain. These different catalysts have been characterized by CO-stripping.

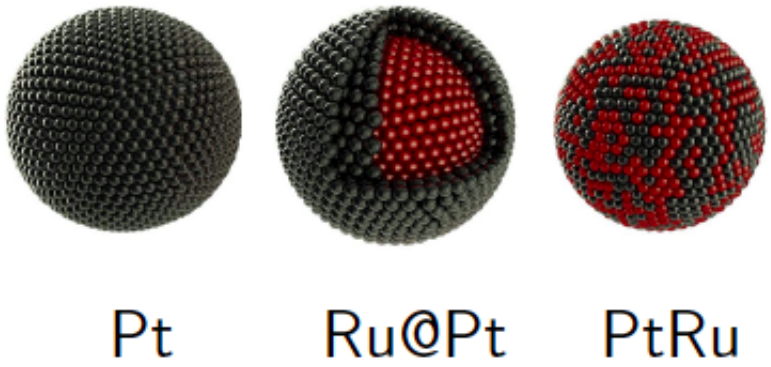

Figur 2.3: Illustration of nanoparticle catalysts. Taken from [3]

.

Figure 2.4 shows the voltammograms of CO-stripping on PtRu, Ru@Pt and Pt nanoparticle catalysts. We see significant differences between the catalysts from these voltammograms. The onset potentials of CO-oxidation are 0.45 V, 0.50 V and 0.70 V, and peak potentials are 0.50 V, 0.58 V and 0.78 V respectively. This agrees with the previous theory of water dissasociation. However, chronoamperometry has shown that in spite of a lower potential for CO-oxidation, the core-shell catalyst is not much better than the Pt-catalyst [8]. It is believed that this may be because of a shift from the serial pathway to the parallell pathway from reaction 2.2 [3].

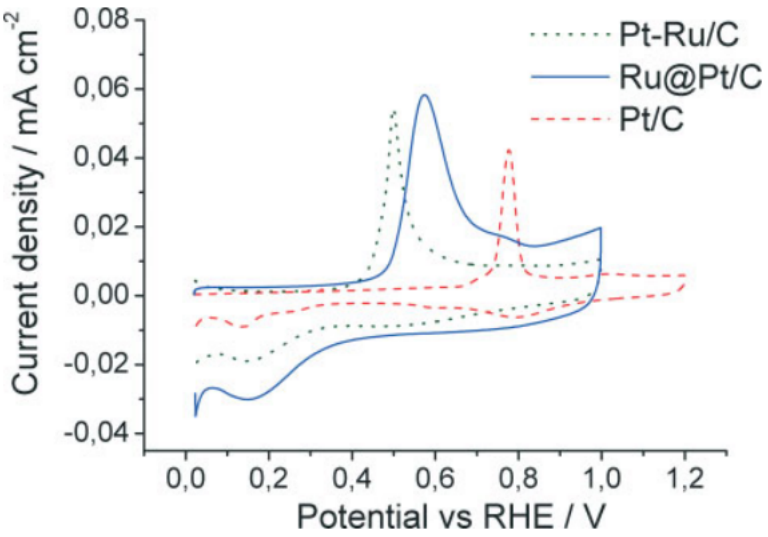

Figur 2.4: 10 mV/s stripping voltammetry of an adsorbed layer of CO(ads) at a Pt-Ru/C alloy, Ru@Pt/C core-shell, and Pt/C catalysts. The CO(ads) layer was formed by purging the electrolyte (0.5 M HClO4) with CO(g) at 0.05 V for 2 min followed by 30 min of Ar(g) purging. Taken from [9].

3. Experimental

3.1 Electrodes

The electrodes used were gold and platinum disk electrodes, ring-disk assemblies with gold or platinum ring electrodes and disk inserts of platinum or glassy carbon. All these electrodes were encased in teflon and manufactured by Pine Instruments. Both the disk electrodes and the disk-insert electrodes had a diameter of 5 mm, and the ring had a inner diameter of 6.5 mm and an outer diameter of 7.5 mm. The palladium electrode were manufactured by using a 0.5 mm in diameter palladium wire (Alfa Aesar Premion 99.99+%) and encasing it in a glass tube which were sealed at the bottom to create a reproducable surface. The electrodes were polished with 0.05 µm alumina particles on a polishing cloth and rinsed in nanopure water (MilliQ) between experiments. They were polished with 5 µm and 0.3 µm alumina particles when needed. The electrode for the AFM (atomic force microscope) microcell was made by using a glass plate with a gold foil on top. Taking a piece of scotch tape with a circular hole in and taping it on the gold foil to get a defined surface to use the catalyst on.

3.2 Catalyst

The catalyst was prepared by using the method described by Garsany et. al. [10]. The ink for platinum catalyst was prepared by measuring 1 µg of 20 % Pt-loading on carbon black (Alfa Aesar) and then adding 1 mL of nanopure water and 20 µL Nafion solution (5 % D-520 Alfa Aesar). For the core-shell catalyst, 1.60 µg of Ru@Pt

nanoparticles was used to get the same platinum loading as the Pt-ink. The catalyst for the AFM electrochemical cell was made by using 2 µg of 20 % Pt-loading on carbon black and then adding 0.8 mL of nanopure water, 0.2 mL isopropanol and 20 µL Nafion solution. The solution was then ultrasonicated for 30 minutes before a 20 µL droplet was pipetted onto a glassy carbon electrode in a ring-disk assembly. For the AFM electrochemical cell, 30 µL of the ink was pipetted onto to gold foil. These were then placed in a glass dome with a low flow of nitrogen gas for at least 45 minutes to dry.

3.3 Electrochemical characterizing

The electrochemical cell used for most of the experiments is a glass cell with five openings. A glass frit was used to introduce glass to the cell, both in the solution and above. A water valve was used to prevent gas flow into the cell. The counter electrode was made of a platinum foil. The reference electrode was a glass tube with a platinum mesh seperated from the solution by a glass tip. It was prepared by filling the inner tube with 0.1 M $HClO_4$ (Merch Chemicals, 70 %) and connected to a platinum counter electrode in the same solution. Then a potential of 4 V was applied by using a potentiostat (Agilent E3633A) until the tube was halfway filled with H_2 gas.

The base electrolyte was made by making a 200 mL solution of 0.1 M $HClO_4$. $HClO_4$ was used because ClO_4^- has been shown to adsorb less on platinum, platinum-based catalysts and palladium than e.g. SO_4^-, so we get more activity and higher current with ClO_4^- [10]. Experiments were performed in this base electrolyte with 1 M CH_3OH (Acros Organics, 99.8 %) and different concentrations of HCOOH (Sigma Aldrich, 96 % ACS) or HCHO (Sigma Aldrich, 37 %, stabilised in 10 - 15 % methanol).

All experiments were performed at room temperature with the same potentiostat (AUTOLAB) and software (NOVA). Argon was bubbled through the solution for 30 minutes before the experiments to eliminate the oxygen, and set to flow above the solution afterwards. All potentials are set against the reversible hydrogen electrode (RHE). Before experiments, the electrodes were cycled to activate the surface or catalyst and achieve a stable voltammogram.

Figur 3.1: Electrochemical setup used in most experiments

The experiments for characterizing the ring-electrodes for different concentrations of formaldehyde and formic acid were performed by activating them in the base electrolyte, adding methanol to 1 M to get a baseline, and then adding formaldehyde or formic acid to get concentrations of 10^{-6} M up to 1 M. The CV was performed from potentials of 0.05 V to 1.6 V at sweep rates from 10 mV/s to 150 mV/s and with rotation speed from 400 RPM to 2000 RPM.

For the palladium electrode and deposited layers, experiments were performed in the same solutions but different potentials on CV, 0.4 V to 1.2 V. This was to prevent formation of hydrous oxide from the hydrogen absorption in palladium below 0.4 V [11], and to prevent the formation of PdO_2 which forms above 1.4 V, and also to prevent dissolution of palladium [12]. The hydrous oxide will change the composition of the palladium electrode and this can affect the results. The PdO_2 have to prevented because methanol oxidation is active on this oxide [13].

3.4 Ring-disk experiments

The ring-disk experiments were performed in a 0.1 M $HClO_4$, 1 M CH_3OH solution. The disk electrodes were plane platinum, platinum catalyst on glassy carbon and Ru@Pt core-shell catalyst on glassy carbon. Both ring and disk electrodes were activated in a 0.1 M $HClO_4$ solution before methanol was added. The disk was set to a constant potential of 1.0 V where the MOR is active. Rotation was 700 RPM for these experiments. At different time intervals, CV was performed on the ring with sweep rate of 100 mV/s and 10 mV/s, and the potential was held at 0.4 V between the CVs.

3.5 Electrodeposition

Palladium was electrodeposited on platinum ring and disk and on gold disk electrodes based on a paper by F. Sarto et. al. [14]. Only three different electrodes were used, and these was polished between every deposition. The electrodes were first cleaned in a 0.1 M $HClO_4$ solution by cycling the electrodes 50 times from 0.05 V to 1.4 V for platinum and 0.05 V to 1.6 V for gold. Then a solution with 1 M HCl (Merch Chemicals, 37 %) and 10 mM $PdCl_2$ (Alfa Aesar, Premion 99.999 %) were made. In this solution, galvanostatic electrodeposition was done by setting a constant current and a set time for deposition. Several different parameters were used, as can be seen in table 3.1. The charge was calculated by using the equation:

$$Q_{ED} = i \times t \times \eta \tag{3.1}$$

where η is the efficiency, and assuming that the reaction:

$$Pd^{2+} + 2e^- \rightarrow Pd^0 \tag{3.2}$$

is 100 % effective. The nominal load can be calculated by Faraday's law:

$$L_{ED} = Q_{ED} \times \frac{Mm}{F \times n} \tag{3.3}$$

where $Mm = 106.42$ is the molar mass of palladium, $F = 96485C/\text{mol}$, the Faraday constant, and $n = 2$ is the number of electrons involved in the reaction.

Tabell 3.1: Electrodeposition on platinum disk (EDPtD1 - EDPtD10), platinum ring (EDPtR1 - EDPtR2) and gold disk electrode (EDAuD11 - EDAuD13).

Sample	Current [mA cm^{-2}]	Time [s]	Charge [mC cm^{-2}]	Nom. Pd load [µg cm^{-2}]	Rotation	Surface
EDPtR1	5.1	250	1275	703	0 RPM	Black, even layer
EDPtR2	5.1	250	1275	703	0 RPM	Black, even layer
EDPtD1	5.1	250	1275	703	0 RPM	Even layer
EDPtD3	5.1	250	1275	703	0 RPM	Uneven layer, spots
EDPtD4	2.55	500	1275	703	0 RPM	Uneven layer, spots
EDPtD5	2.55	1000	2550	1406	0 RPM	Black, even layer
EDPtD6	0.51	250	127.5	70.3	0 RPM	Even layer
EDPtD8	5.1	50	255	140.6	1000 RPM	Black, even layer
EDPtD9	0.51	250	127.5	70.3	1000 RPM	Even layer
EDPtD10	1.28	250	320	176.5	1000 RPM	Grey, even layer
EDAuD11	5.1	250	1275	703	1000 RPM	Black, even layer
EDAuD12	0.51	250	127.5	70.3	1000 RPM	Grey, even layer
EDAuD13	0.051	1000	51	28.1	1000 RPM	Thin layer, hint of gold

3.6 Microcell

A microcell was improvised by using an electrochemical cell designed for AFM. One of the electrodes were as described in section 3.2. The other electrode used were the palladium wire in glass. These electrodes were interchanged as work and counter electrode. The gold plate was connected to the cell by using a palladium wire in contact with the gold foil outside the cell. The reference electrode used were the same as described in section 3.3, but only the inner tube was used directly in the solution.

The experiment was performed by adding 700 µL of 0.1 M $HClO_4$ solution to the cell and activating the catalyst by cycling it from 0.05 V to 1.2 V at 100 mV/s. Then 1 M methanol was added and CV were perfomed on the palladium electrode from 0.4 V to 1.2 V at 100 mV/s and 10 mV/s to generate a baseline voltammogram. Then the palladium catalyst electrode was set to constant potential of 1 V for 40 minutes. After this, CV was performed again on the palladium electrode at 10 mV/s, 100 mV/s and 200 mV/s.

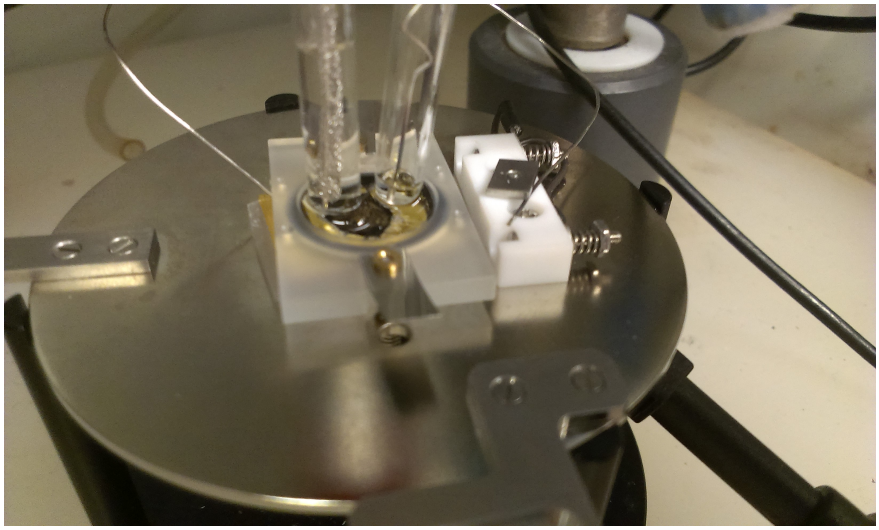

Figur 3.2: Microcell setup

This setup was used to have a small volume so that the biproducts could build up a significant concentration that could be detected by palladium electrode.

4. Results

4.1 Modeling of concentration

4.1.1 Laplace Transform

Laplace transforms are often used to solve difficult differential equations in an much easier manner. It works by taking a problem that is difficult to solve in t, transform it to an equation in s that is easier to solve than the equation in t. When this is solved, the inverse laplace transform, $\mathcal{L}^{-1}$, is used to get a solution in t. The laplace transform is defined as:

$$\mathcal{L}\left\{F(t)\right\} = \int_0^\infty e^{-st} F(t) dt = \tilde{f}(s) \tag{4.1}$$

To solve the later equations we need some rules for the laplace transform. First the laplace transform of the derivative of f.

$$\mathcal{L}(f') = s\mathcal{L}(f) - f(0) \tag{4.2}$$

And to simplify the calculations we can define the easiest laplace transform:

$$\mathcal{L}(C) = \frac{C}{s} \tag{4.3}$$

4.1.2 Concentration

To determine if this method of detection of byproducts from the methanol reaction is viable, we want to calculate approximately what concentrations of formaldehyde and

formic acid we could expect to find at the ring in the ring-disk electrode setup. The most precise way to solve this would be to solve the following steady-state convective-diffusion equation where r is the radial coordinate on the disk and x is the distance from the planar surface. We use R to descripe the species we are interested in:

$$v_r \left(\frac{\partial C_R}{\partial r} \right) + v_y \left(\frac{\partial C_R}{\partial x} \right) = D_R \left(\frac{\partial^2 C_R}{\partial x^2} \right) \tag{4.4}$$

This equation is too hard for us to solve for our system, so we will use an simpler approximation. To solve this we envision a volume element at the edge of the disk. At $t = 0$, there will be a steady state with production of species R and a concentration gradient of R. At $t > 0$ this volume element will travel from the disk to the ring without any more production of species R.

This is modeled by seeing it as a potential step experiment where the potential is changed from E_1 where the reaction occurs, to a potential, E_2, with no reaction. This is modeled by using Fick's second law of diffusion:

$$\frac{\partial C_R(x,t)}{\partial t} = D_R \left(\frac{\partial^2 C_R(x,t)}{\partial x^2} \right) \tag{4.5}$$

under the boundary conditions:

$$\lim_{x \to \infty} C_R(x,t) = 0 \tag{4.6}$$

$$C_R(x,0) = C_R^i(x) = C_R^0 e^{-Bx} \tag{4.7}$$

$$\frac{\partial C_R}{\partial x} = 0; t > 0, x = 0 \tag{4.8}$$

where $C_R^i(x)$ is the aproximation of the initial concentration gradient, C_R^0 is the initial concentration at the electrode surface and B is a constant determined by the thickness of the diffusion layer for R. This problem can be solved by using the laplace transform (4.1). By applying (4.5) to (4.2) we get:

$$\begin{aligned} \mathcal{L}\left\{ \frac{\partial C_R(x,t)}{\partial t} \right\} &= s\tilde{C}_R(x,s) - C_R(x,0) = D_R \frac{\partial \tilde{C}_R(x,s)}{\partial x^2} \\ \mathcal{L}\left\{ \frac{\partial C_R(x,t)}{\partial t} \right\} &= s\tilde{C}_R(x,s) - C_R^0 e^{-Bx} = D_R \frac{\partial \tilde{C}_R(x,s)}{\partial x^2} \end{aligned} \tag{4.9}$$

From this we get the nonhomogeneous ODE:

$$D_R \frac{\partial \tilde{C}_R(x,s)}{\partial x^2} - s\tilde{C}_R(x,s) = -C_R^0 e^{-Bx} \tag{4.10}$$

This can be solved by first finding a general solution for the homogeneous ODE, $\tilde{C}_R^h(x,s)$, and then a prticular solution for the nonohomogeneous ODE, $\tilde{C}_R^p(x,s)$ so that:

$$\tilde{C}_R(x,s) = \tilde{C}_R^h(x,s) + \tilde{C}_R^p(x,s) \tag{4.11}$$

First we find a homogeneous solution:

$$\tilde{C}_R^h(x,s) = A(s)e^{\lambda x} \tag{4.12}$$

where $A(s)$ is a variable only in s. We check and see if this is a valid solution and find an expression for λ:

$$\frac{\partial \tilde{C}_R^{h2}(x,s)}{\partial x^2} = A(s)\lambda^2 e^{\lambda x} \tag{4.13}$$

$$D_R \frac{\partial \tilde{C}_R^{h2}(x,s)}{\partial x^2} = s\tilde{C}_R^h(x,s) \tag{4.14}$$

$$D_R \lambda^2 A(s)e^{\lambda x} = sA(s)e^{\lambda x} \tag{4.15}$$

$$\lambda^2 = \frac{s}{D_R} \tag{4.16}$$

$$\lambda = \pm\sqrt{\frac{s}{D_R}} \tag{4.17}$$

From (4.6) we see that the concentration is 0 at infinite x, so λ have to be negative.

Next we find the particular solution

$$\tilde{C}_R^p(x,s) = K\exp(-Bx) \tag{4.18}$$

and a solution for the constant K:

$$\frac{\partial \tilde{C}_R^{p2}(x,s)}{\partial x^2} = KB^2\exp(-Bx) \tag{4.19}$$

$$D_R \frac{\partial \tilde{C}_R^{p2}(x,s)}{\partial x^2} - s\tilde{C}_p^h(x,s) = -C_R^0\exp(-Bx) \tag{4.20}$$

$$KB^2 D_R\exp(-Bx) - sK\exp(-Bx) = -C_R^0\exp(-Bx) \tag{4.21}$$

$$K = \frac{C_R^0}{s - DB^2} \tag{4.22}$$

and we get:

$$\tilde{C}_R(x,s) = A(s)\exp\left(-\sqrt{\frac{s}{D_R}}x\right) + \frac{C_R^0\exp(-Bx)}{s - DB^2} \tag{4.23}$$

We then use the boundary condition for the concentration gradient at $x = 0, t > 0$ from (4.8) to fix $A(s)$:

$$\frac{\partial C_R(x,s)}{\partial x}_{x=0} = -A(s)\sqrt{\frac{s}{D_R}}\exp\left(-\sqrt{\frac{s}{D_R}}x\right) - \frac{C_R^0 B\exp(-Bx)}{s - DB^2} = 0 \tag{4.24}$$

$$A(s) = -\frac{C_R^0 B\sqrt{D_R}}{(s - DB^2)\sqrt{s}} \tag{4.25}$$

Put into (4.23) we get:

$$\tilde{C}_R(x,s) = \frac{C_R^0}{s - DB^2}\left\{\exp(-Bx) - B\sqrt{\frac{D_R}{s}}\exp\left(-\sqrt{\frac{s}{D_R}}x\right)\right\} \tag{4.26}$$

This equation is too hard to inverse laplace transform, but if we assume we need an equation for short values of t, then we can simplify the equation, because short values of t means large values of s. Then we get:

$$\tilde{C}_R(x,s) = \frac{C_R^0}{s}\left\{\exp(-Bx) - B\sqrt{\frac{D_R}{s}}\exp\left(-\sqrt{\frac{s}{D_R}}x\right)\right\} \tag{4.27}$$

This equation can be inverse laplace transformed, and we get the solution:

$$C_R(x,t) = C_R^0\left\{\exp(-Bx) + Bx - \frac{2B\sqrt{D_R t}}{\sqrt{\pi}}\exp(-\frac{x^2}{4D_R t}) - Bx\ \mathrm{erf}\left(\frac{x}{2\sqrt{D_R t}}\right)\right\} \tag{4.28}$$

Now we need to find the initial concentration, C_R^0, the constant B and the transit time our volume element will use to travel from the edge of the disk to the ring.

The transit time can be calculated by the formula [15]:

$$t = 3.58\omega^{-1}\left(\frac{\nu}{D_R}\right)^{1/3}\left\{\log\left(\frac{r_2}{r_1}\right)\right\}^{2/3} \tag{4.29}$$

where ω is the rotation speed in radians per second and ν is the kinematic viscosity.

4.1.3 Initial concentration

To calculate the initial concentration of species R we use the fact that the rate of consumption must equal the rate of production. Our reaction is:

$$\mathrm{CH_3OH} \rightarrow X_A\mathrm{HCOOH} + X_B\mathrm{HCHO} + X_C\mathrm{CO_2} + ne^- \tag{4.30}$$

where X_i is the fraction of their respective species produced from CH_3OH. Formic acid, formaldehyde and carbon dixoide formation is respectively a 4-, 2- and 6-electron reaction. n is given by the mol fractions and electron transfer number for these:

$$n = 4X_A + 2X_B + 6X_C \tag{4.31}$$

Using formic acid as an example, the mol flux is:

$$X_A j_{\mathrm{CH_3OH}} = -j_{\mathrm{HCOOH}} \tag{4.32}$$

The mol flux can be related to the current density by:

$$j = D\frac{\partial C}{\partial x} = \frac{i}{nF} \tag{4.33}$$

We can combine these expressions and get:

$$X_A \frac{i_{\mathrm{CH_3OH}}}{nF} = -D_{\mathrm{HCOOH}} \frac{\partial C_{\mathrm{HCOOH}}}{\partial x} = -D_{\mathrm{HCOOH}} \frac{C^b_{\mathrm{HCOOH}} - C^s_{\mathrm{HCOOH}}}{\delta_{\mathrm{HCOOH}}} \tag{4.34}$$

Where C^b is the bulk concentration, C^s is the surface concentration and δ is the diffusion layer thickness. The bulk concentration for formic acid is zero, and the surface concentration is then.

$$C^s_{\mathrm{HCOOH}} = X_A \frac{i_{\mathrm{CH_3OH}} \delta_{\mathrm{HCOOH}}}{nF D_{\mathrm{HCOOH}}} \tag{4.35}$$

To find the diffusion layer thickness we use the results of the diffusion-layer model for RDE [15]:

$$\delta = 1.61 D^{1/3} \omega^{-1/2} \nu^{1/6} \tag{4.36}$$

The constant B can be derived from the model for the concentration gradient and the derivative of (4.7) when x = 0 since the diffusion layer is the the length where the concentration would reach the bulk value if the gradient was constant from x = 0.

$$\frac{\partial C}{\partial x} = \frac{C^s - C^b}{\delta} = -BC^0 \tag{4.37}$$

The bulk concentration is zero and the surface concentration and the start concentration are equal at the surface. At the surface, x is zero and we get:

$$B = \frac{1}{\delta} \tag{4.38}$$

4.1.4 Numerical value

The value we want to find is the concentration on the surface after the transit time, so with $x = 0$, (4.28) reduces to:

$$C_R(0,t) = C_R^0 \left\{ 1 - \frac{2B\sqrt{D_R t}}{\sqrt{\pi}} \right\} \tag{4.39}$$

When we insert the equations for B and t, we get:

$$C_R(0,t) = C_R^0 \left\{ 1 - 1.33 \left[\log\left(\frac{r_2}{r_1} \right) \right]^{1/3} \right\} \tag{4.40}$$

From this result we can see that apart from the initial concentration at $x = 0, t = 0$, the only thing that influences the concentration at the ring is the geometry of the ring-disk electrode. For our ring-disk electrode, the disk have an outer diameter of 5 mm, and the ring have an inner diameter of 6.5 mm, with these values we get that:

$$C_R^{\text{ring}} = 0.36 C^0 \tag{4.41}$$

From later results we have a current and current density, $I_{MeOH} = 2.2mA, i_{MeOH} = 0.011A/cm^2$ at a glassy carbon electrode with platinum catalyst at a rotation of 1000 RPM, or $\omega = 104.72s^{-1}$. To get an approximation for the current efficiencies in (4.30) we use data from Ota, K. et. al. [16]. In their experiments the current efficiency for formic acid, formaldehyde and carbon dioxide were initially 30, 12 and 58 percent respectively. Transformed to mol fractions, we get 32, 26 and 42 percent, and thus $n = 4.32$. Our diffusion coeffecients are $D_{\text{CH}_3\text{OH}} = 1.66 \times 10^{-5} cm^2/s$, $D_{\text{HCOOH}} = 1.52 \times 10^{-5} cm^2/s$ and $D_{\text{HCHO}} = 1.81 \times 10^{-5} cm^2/s$ [17]. The kinematic viscocity is: $\nu = 0.0091 cm^2/s$. All values are at 25 °C.

First we want to calculate the concentration of formic acid. Using the values above, first we calculate the diffusion layer thickness for formic acid using (4.36), $\delta_{\text{HCOOH}} = 1.78 \times 10^{-3} cm$. Then the initial concentration from (4.35): $C^s_{\text{HCOOH}} = 9.90 \times 10^{-7} mol/cm^2 = 9.90 \times 10^{-4} M$. From this we get $C^{\text{ring}}_{HCOOH} = 3.56 \times 10^{-4} M$. The same calculations for formaldehyde gives: $C^{\text{ring}}_{HCHO} = 2.56 \times 10^{-4} M$.

4.2 Ring-disk measurements on gold ring

Figure 4.1 shows the ring-disk experiment on a plane Pt-electrode disk and a gold ring. Four sets of voltammograms were recorded at 100 mV/s and 10 mV/s sweeprate at 700 RPM. Only the results for 100 mV/s sweep rate are shown. First a baseline at no potential on the disk were recorded. Then three voltammograms with 1 V potential on the disk. One from the beginning, then a pause of five minutes before the second one, and then a ten minutes pause before the last one. On figure (a) we see the voltammogram for the gold ring at 10 mV/s with almost identical shapes with an increase in current after 1.2 V, and an cathodic peak at 1.2 V. The difference between the shapes are the slight increase in current form the baseline voltammogram at 1.1 V to 1.4 V. This increase corresponds to the current in figure (b), with the one at 8 minutes have the higher current, with the same correspondence for the others. There is also a slight increase in the cathodic current at the peak and a slight difference at low potentials.

Figure 4.2b shows the current-time relationship at the platinum electrode at a potential of 1.0 V. We see that the current drops sharply at det beginning before it stabilises somewhat. We see that there is a lot of noise in the measurement at times where no CVs were performed at the disk (around 1000 seconds and 2000 - 2500 seconds). There are also some slight zig-zag pattern in the curve.

Figure 4.2 shows the ring-disk experiement with a Pt/C catalyst on glassy carbon disk electrode. Five sets of voltammograms were recorded at 100 mV/s and 10 mV/s at 700 RPM. First the baseline at no potential on the disk. Then four voltammograms with 1 V potential on the disk. One at the beginning, the next after a pause of ten minutes, then another one after another ten minutes pause, and the last one after a twenty minute pause. On figure (a) we see that these voltammograms has approximately the same shape, except that they are shifted to higher values in the order they were recorded. There is also a distortion of the voltammograms.

Figure 4.2b shows the current-time relationship on the Pt/C catalyst electrode. The current drops sharply at the beginning, and continues to drop, altough less steeply at longer times. There are also some noise in the measurements at ca 1500 seconds.

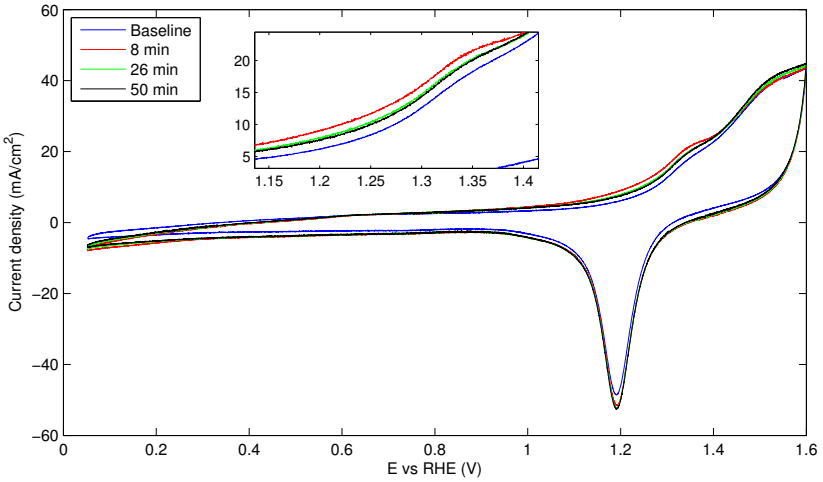

(a) CVs at different times on gold ring electrode. Sweep rate at 10 mV/s

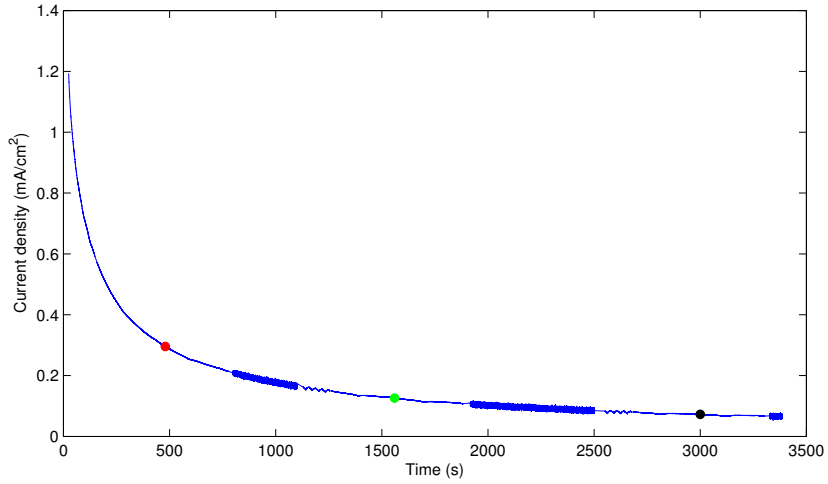

(b) Current vs time on platinum disk. Dots indicate the times the CVs were recorded.

Figur 4.1: Voltammograms and time vs current for a set of measurements in 0.1 M $HClO_4$ and 1 M methanol solution. 700 RPM rotation and a constant potential on a plane platinum disk of 1.0 V.

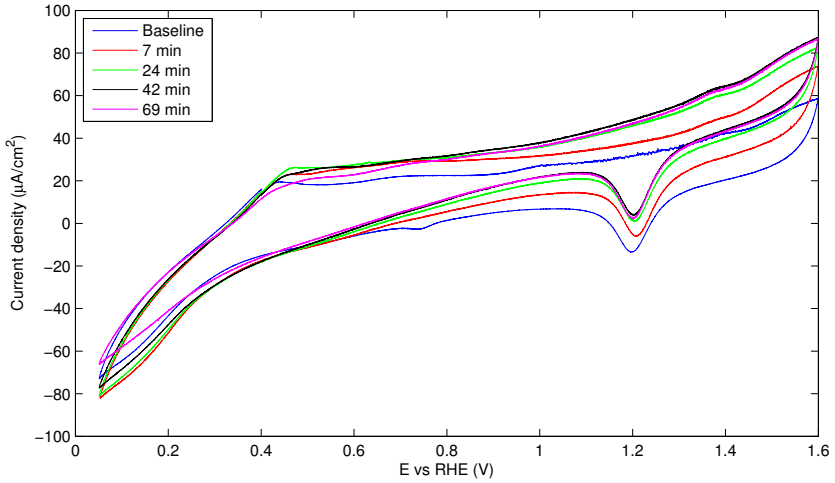

(a) CVs at different times on gold ring electrode. Sweep rate at 10 mV/s

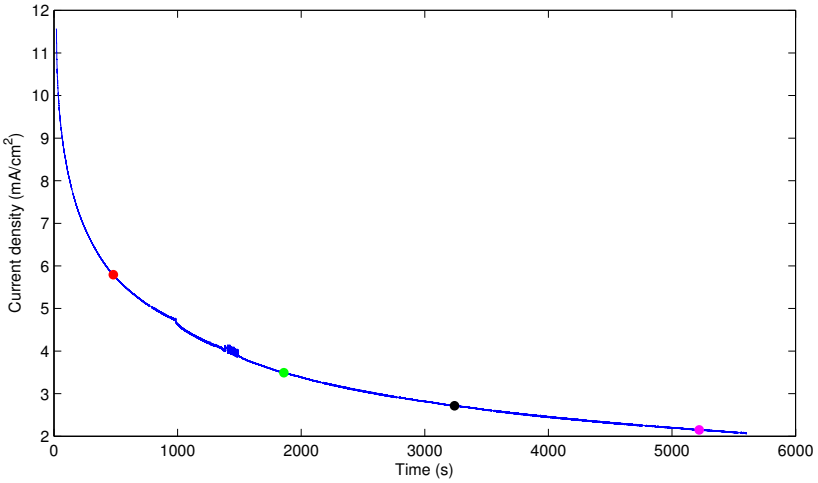

(b) Current vs time on Pt/C catalyst on glassy carbon electrode. Dots indicate the times the CVs were recorded.

Figur 4.2: Voltammograms and time vs current for a set of measurements in 0.1 M $HClO_4$ and 1 M methanol solution. 700 RPM rotation and a constant potential on Pt/C catalyst on a glassy carbon disk of 1.0 V.

4.3 Concentration

In figure 4.3 we have the voltammograms at 10 mV/s for different concentrations of formic acid in a 1M methanol, 0.1 M $HClO_4$ solution on a gold ring electrode at 1000 RPM. Figure (a) shows concentrations from 0 M to 0.1 M, but the lower concentrations are hard to differenciate, so we use figure (b) for these. For the forward scan we see the onset potential from 0.6 to 0.9 potential, with higher potential for lower concentrations of formic acid. 0.1 M have a small peak at 1 V, and 0.01 M and 0.001 M have a plateu here. All formic acid concentrations have a peak at around 1.4 V, slighty shifted to higher potentials for 0.001 M - 0.1 M. On the downward sweep, there is a cathodic peak at 1.2 V for lower concentrations, which is increasing slightly for 10^{-6} M - 10^{-4} M. This peak is almost gone for 0.1 M and 0.01 M. At 1.05 V there is a slight peak for lower concentrations that increases rapidly for 0.001 M and above. At low potentials the zero concentration and 0.001 M voltammograms have a cathodic current.

Figure 4.4 shows the voltammograms at 10 mV/s for different concentrations of formaldehyde in a 1M methanol, 0.1 M $HClO_4$ solution on a gold ring electrode at 1000 RPM. Figure (a) shows the concentrations from 0M to 0.1 M, and figure (b) shows only the lower concentrations to see these more clearly. For 0.01 M and 0.1 M we see a clear peak at 1.35 V and a smaller peak on the downward sweep at 1.1 V. At lower concentrations there are a slightly higher current for 0.001 M from 1.1 V, and for the lower concentrations from 1.3 V compared to the baseline. These concentrations also have a higher cathodic peak than the baseline at ca 1.2 V. And the baseline have a slightly cathodic current at low potentials.

Figure 4.5 shows the voltammograms at 10 mV/s for different concentrations of formic acid on a platinum disk at 1000 RPM in a 1M methanol, 0.1 M $HClO_4$ solution. In figure (a) we see that 0.1 M has a peak at 0.55 V at forward sweep and a slight shoulder at 0.55 V for the downward sweep. 0.01 M also has a slighty earlier onset potential for forward sweep and and activity further towards lower potentials than the baseline. In figure (b) we see that except for 0.001 M, the sweeps are almost identical, and a slightly misshaped forward peak for 0.001 M.

In figure 4.6 we have the voltammograms at 10 mV/s on a palladium wire electrode for different concentrations of formic acid in a 1M methanol, 0.1 M $HClO_4$ solution. In figure (a) we see the steady decrease of activity in the forward sweep for 0.1 M and 0.01 M. From both (a) and (b) we see that all concentrations have a peak at

0.75 V on the downward sweep and all except 0.1 M at 0.85 V for the forward sweep. The lower concentrations have a slightly higher current over the entire sweep than the baseline of 0 M.

Figure 4.7 shows the voltammograms at 10 mV/s on a palladium wire electrode for different concentrations of formaldehyde in a 1M methanol, 0.1 M $HClO_4$ solution. Except for the large shift from the baseline to $10^{-}6$ M, higher concentrations only yields larger peaks. For low concentration, this is a very low increase. There is also a distortion of the voltammograms.

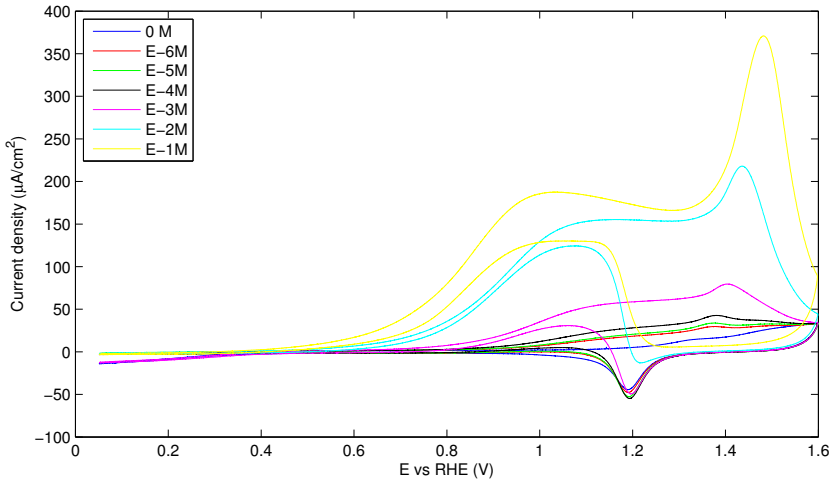

(a)

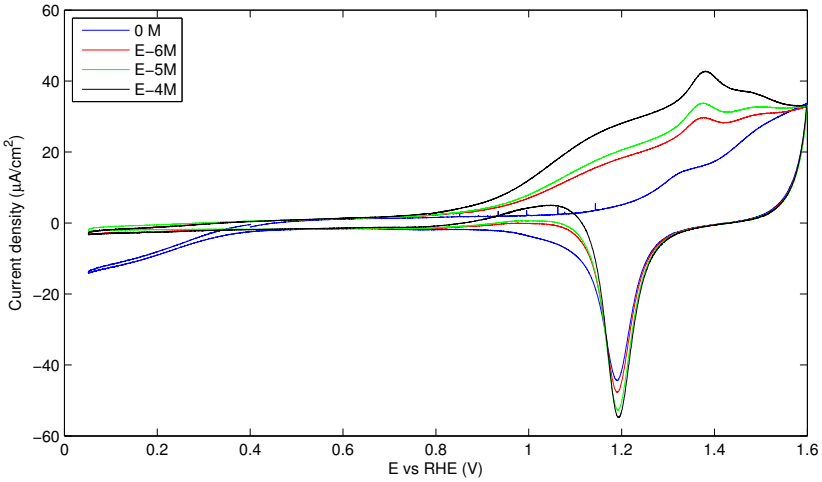

(b)

Figur 4.3: The top figure shows the CV for different concentrations of formic acid in a 1 M methanol, 0.1 M $HClO_4$ solution on a gold ring electrode. Sweep rate of 10 mV/s and rotation of 1000 RPM. The bottom figure is the same with the higher concentrations removed.

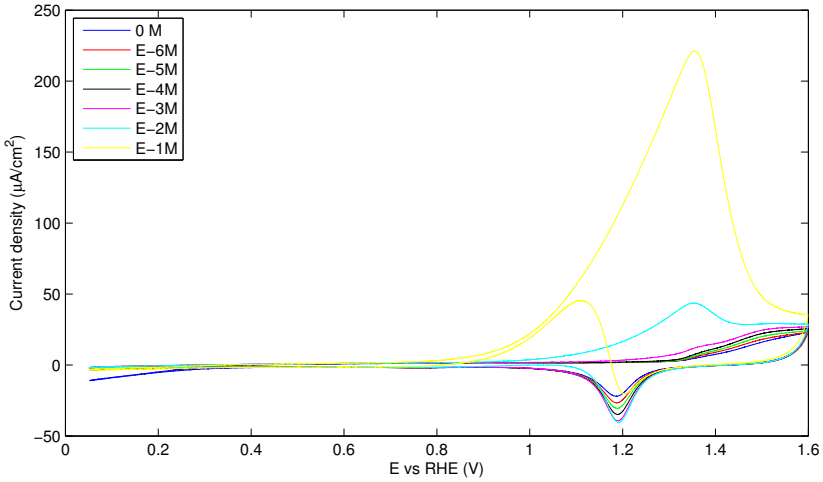

(a)

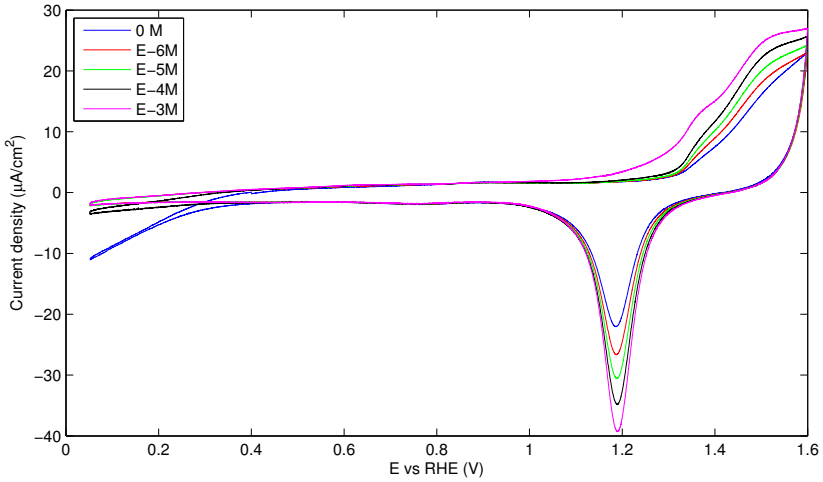

(b)

Figur 4.4: The top figure shows the CV for different concentrations of formaldehyde in a 1 M methanol, 0.1 M $HClO_4$ solution on a gold ring electrode. Sweep rate of 10 mV/s and rotation of 1000 RPM. The bottom figure is the same with the higher concentrations removed.

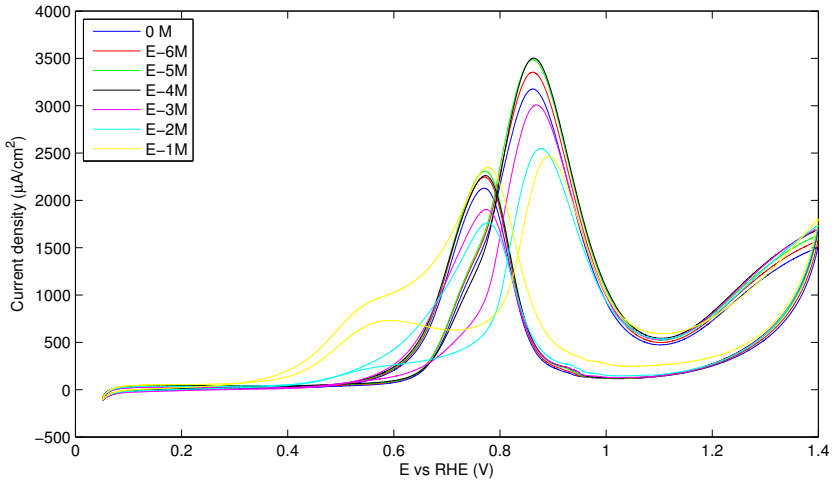

(a)

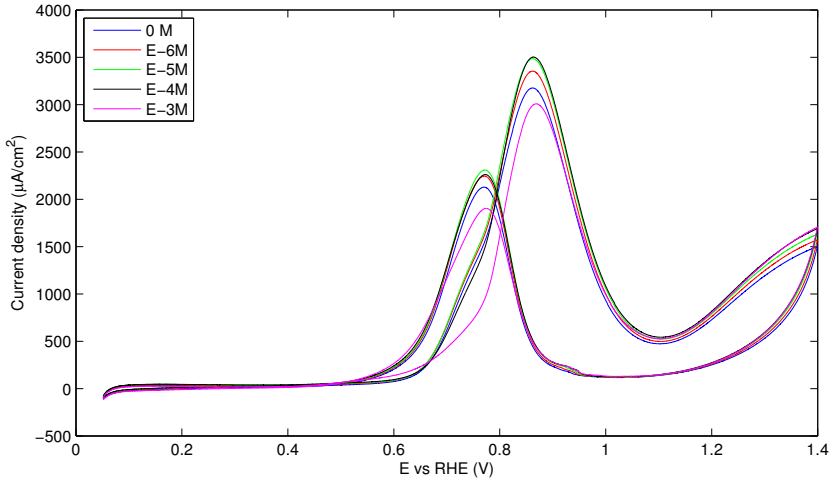

(b)

Figur 4.5: The top figure shows the CV for different concentrations of formic acid in a 1 M methanol, 0.1 M $HClO_4$ solution on a platinum ring electrode. Sweep rate of 10 mV/s and rotation of 1000 RPM. The bottom figure is the same with the higher concentrations removed.

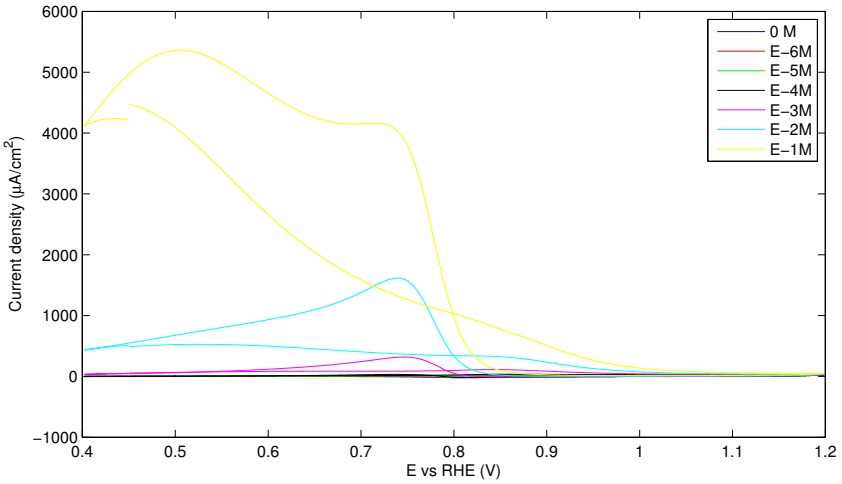

(a)

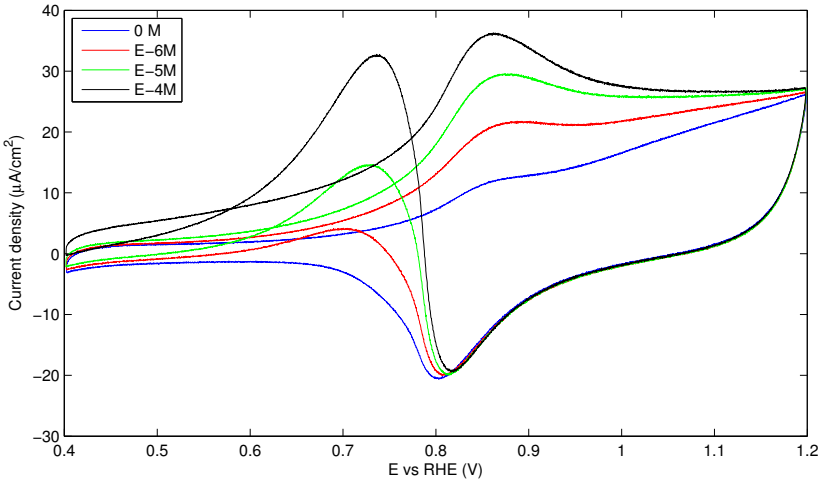

(b)

Figur 4.6: The top figure shows the CV for different concentrations of formic acid in a 1 M methanol, 0.1 M $HClO_4$ solution on a palladium wire. Sweep rate of 10 mV/s. The bottom figure is the same with the higher concentrations removed.

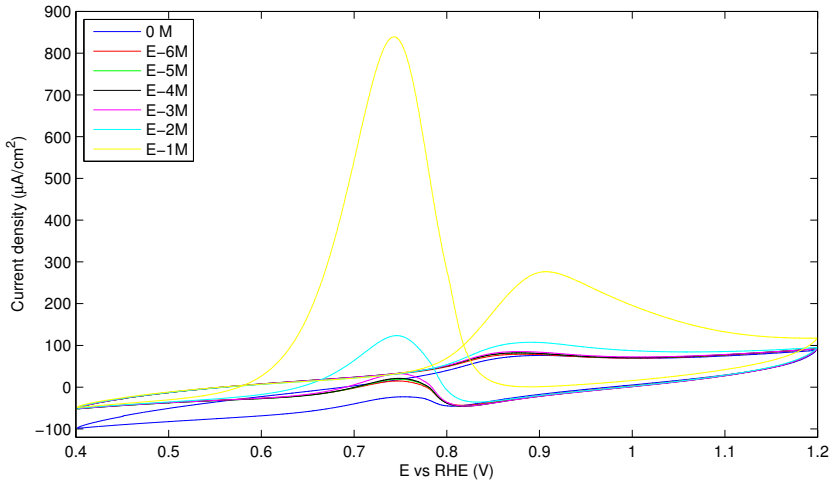

(a)

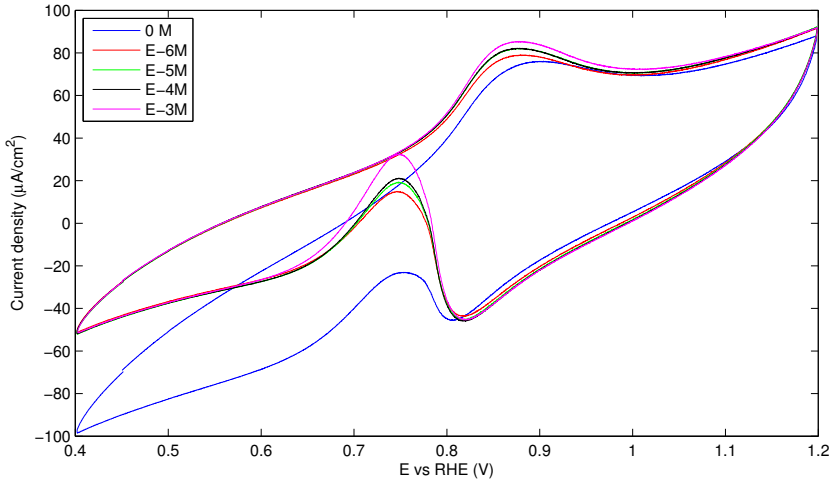

(b)

Figur 4.7: The top figure shows the CV for different concentrations of formic acid in a 1 M methanol, 0.1 M $HClO_4$ solution on a palladium wire. Sweep rate of 10 mV/s. The bottom figure is the same with the higher concentrations removed.

4.4 Palladium electrodeposited electrodes

Figure 4.8 shows the voltammograms after 40 cycles of cleaning at 100 mV/s for before each electrodeposition. We see in (a) that there is a significant difference between EDPtD1 and EDPtR1 and the rest of the samples where the cathodic peak has shifted from around 0.8 V to 0.7 V in addition to an increasingly larger current at low potentials for later samples. In (b) we see a much smaller difference between EDAuD11 and the rest where we have a new peak at 0.6 V and a larger current at low potentials.

Figure 4.9 shows the voltammogram in the palladium solution, 10 mM $PdCl_2$ and 1 M HCl. Beginning at the downward sweep we see cathodic peaks at 0.15 V and 0 V before a long, constant slope up and down, and then anodic peaks at 0.04 V and 0.15 V with very low current above these potentials.

The electrodeposition of palladium onto the electrodes are shown in figure 4.10 where the potential is measured against the time. The figure have been split in two based on the rotation, (a) for 0 RPM and (b) for 1000 RPM, and have been cut of at 250 seconds to get a better look at the relevant part. EDPtR1 is not shown because the relevant data was not recorded. The parameters can be found in table 3.1. We see that EDPtR2, EDPtD4 and EDPtD5 have a potential drop in two stages. For EDPtD1 and EDPtD3 it has hard to say, while EDPtD6 have a gentle slope. EDPtD4 and EDPtD5 has a longer first stage and a higher initial potential than the others, except EDPtD6, and share a lower current of 2.55 $\mathrm{mA\,cm^{-2}}$, compared to 5.1 $\mathrm{mA\,cm^{-2}}$. EDPtD6 has a higher intial potential and less defined stages and a lower current of 0.51 $\mathrm{mA\,cm^{-2}}$.

For the electrodeposition with rotation (b) we have a different slope where the potentials increase until they reach a constant value, except for EDAuD13 which decreases but at a higher potential. For EDPtD10 and EDAuD12 we see a slight decrease at the start before they increase to reach this value. From the parameters we see that after the initial stage they group up according to the current density, and lower current densities gives higher potentials. When comparing the potentials with and without rotation we see that, when the current density is taken into account, we have a lower potential without rotation.

Figure 4.11 shows the voltammograms for the electrodeposited palladium electrodes in 0.1 M $HClO_4$ at 10 mV/s. These are grouped by lowest, (a), to highest, (d),

current density to better see the individual shapes of the voltammograms. Most of the voltammograms have to same basic shape with higher current from 0.7 V and small peaks at around 0.8 V and 1.05 V for the forward sweep and a cathodic peak at around 0.8 V for the backwards sweep. There are some variation of which peak is higher and lower, and a very large variation of current. EDPtD1 (a) and EDPtD5 (c) have a slightly different shapes with no peak at 0.8 V and a higher peak at 1.05 V.

Figures 4.12 and 4.13 shows the voltammograms for the electrodeposited palladium electrodes in 0.1 M $HClO_4$ and 1 M methanol solution at 10 mV/s. These are also grouped as highest (4.12a), medium (4.12b) and lowest activity (4.13). We see that almost all the samples have a high activity in methanol except for EDPtD1 and EDAuD13. In addition, EDPtD5 have no additional activity in methanol solution and has the same shape as in figure 4.11c.

In figure 4.14 we have voltammograms for different concentrations of formic acid in 0.1 M $HClO_4$ and 1M methanol on sample EDPtD1 at 10 mV/s. We see that for 10^{-6} M to 10^{-3} we have a slight increase in current from 0.7 V to 1.05 V for the forward sweep, and an increase in the peak at 0.75 V for backwards sweep. For 0.001 M we see an increase for 0.4 V to 1.05 V and a greater peak at 0.75 V for backwards sweep. CVs were performed for higher concentrations, but these are not shown.

Figure 4.15 shows voltammograms at 100 mV/s on sample EDPd5 in 1 M methanol and 0.1 M $HClO_4$ and formic acid concentration of 0 M, 0.001 M and 0.1 M. The dotted (:) lines are at sweep number 1, striped lines (–) at sweep number 5 and the solid lines (-) at sweep number 10. We can see that all voltammograms are almost identical for different sweeps and concentrations except for 0.1 M where we have significantly higher current for the first sweep than the tenth, where is it almost down to the other sweeps in current.

We can summarize this section by sorting the samples by current density for deposition, palladium loading, current in 0.1 M $HClO_4$ and in 0.1 M $HClO_4$ and 1 M methanol. This is done in table 4.1 and we can see that the currents generally follows the palladium loading on the electrode.

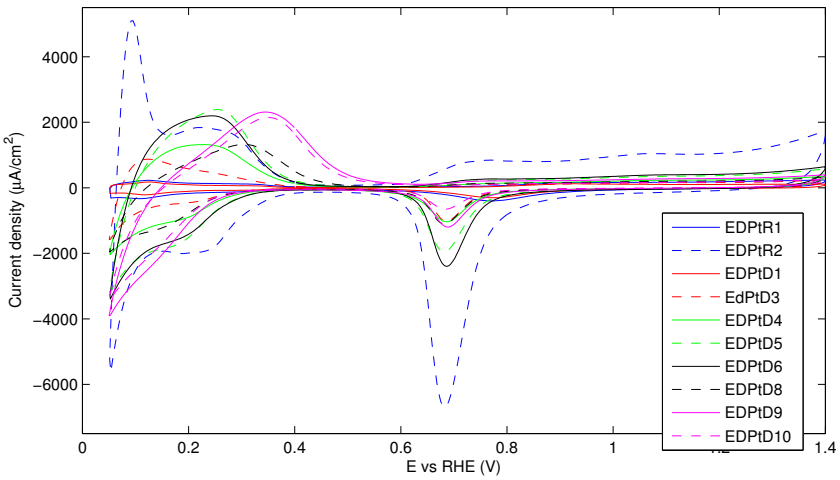

(a) Voltammogram for platinum electrodes

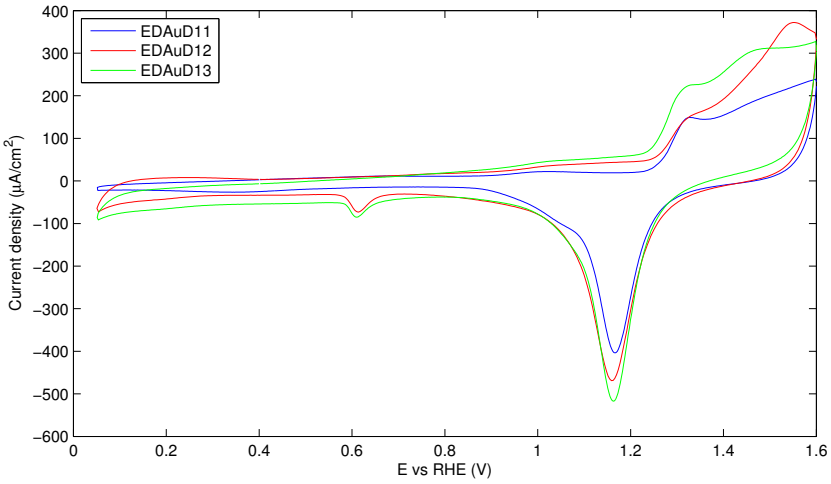

(b) Voltammogram for gold electrodes

Figur 4.8: The figures shows the voltammograms for the cleaning before each electrodeposition. Cycle number 40 at 100 mV/s sweep rate.

Tabell 4.1: Comparison of the electrodeposited palladium electrodes. Sorted from lowest to highest values of current density for deposition, palladium loading, current in 0.1 M $HClO_4$ and in addition of 1 M methanol.

Value dep. curr.	Deposition current density [mA cm^{-2}]	Value Pd load.	Pd loading [µg cm^{-2}]	$HClO_4$	CH_3OH
0.051	EDAuD13	28.1	EDAuD13	EDAuD13	EDPtD5
0.51	EDPtD6	70.3	EDPtD6	EDPtD9	EDPtD1
	EDPtD9		EDPtD9	EDAuD12	EDAuD13
	EDAuD12		EDAuD12	EDPtD1	EDAuD12
1.28	EDPtD10	140.6	EDPtD8	EDPtD10	EDPtD9
2.55	EDPtD4	176.5	EDPtD10	EDPtD6	EDPtD6
	EDPtD5	703	EDPtR1	EPtD4	EDPtD10
5.1	EDPtR1		EDPtR2	EDPtD3	EDPtD4
	EDPtR2		EDPtD1	EDPtR1	EDPtD3
	EDPtD1		EDPtD2	EDPtD8	EDPtR1
	EDPtD3		EDPtD4	EDPtD5	EDPtD8
	EDPtD8		EDAuD11	EDPtR2	EDPtR2
	EDAuD11	1406	EDPtD5	EDAuD11	EDAuD11

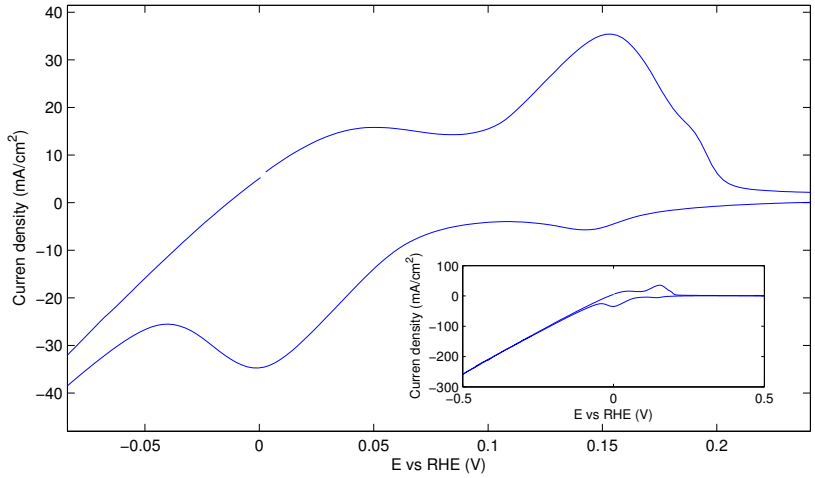

Figur 4.9: Voltammogram recorded on Pt-ring before EDPt1 in 10 mM $PdCl_2$ and 1 M HCl solution at 100 mV/s from -0.5 V to 0.5 V. Main picture of the interesting section, inlay of the whole voltammogram.

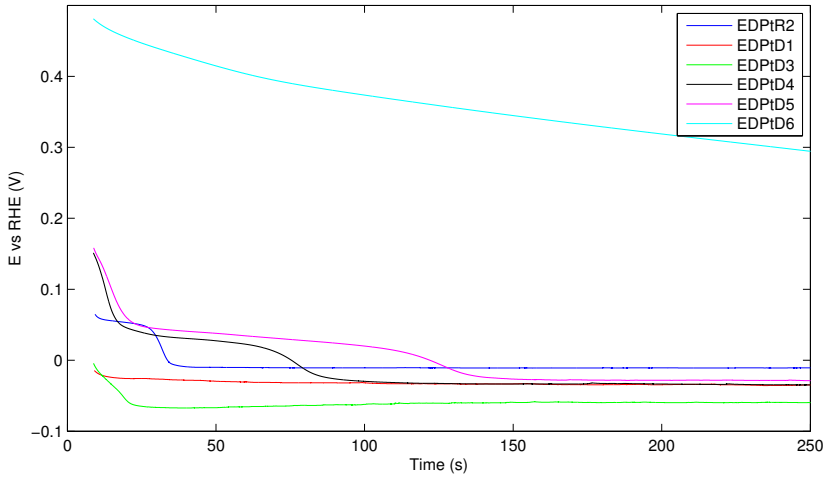

(a) Electrodeposition without rotation

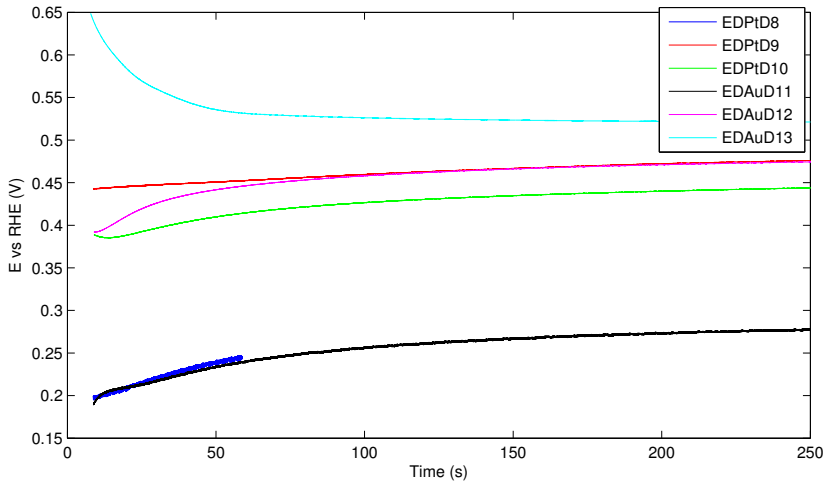

(b) Electrodeposition with rotation

Figur 4.10: The figures shows the galvanostatic electrodeposition the electrodes. Figures have been cut at 250 seconds. The lines are approxemately straight for electrodeposition that lasts longer than this.

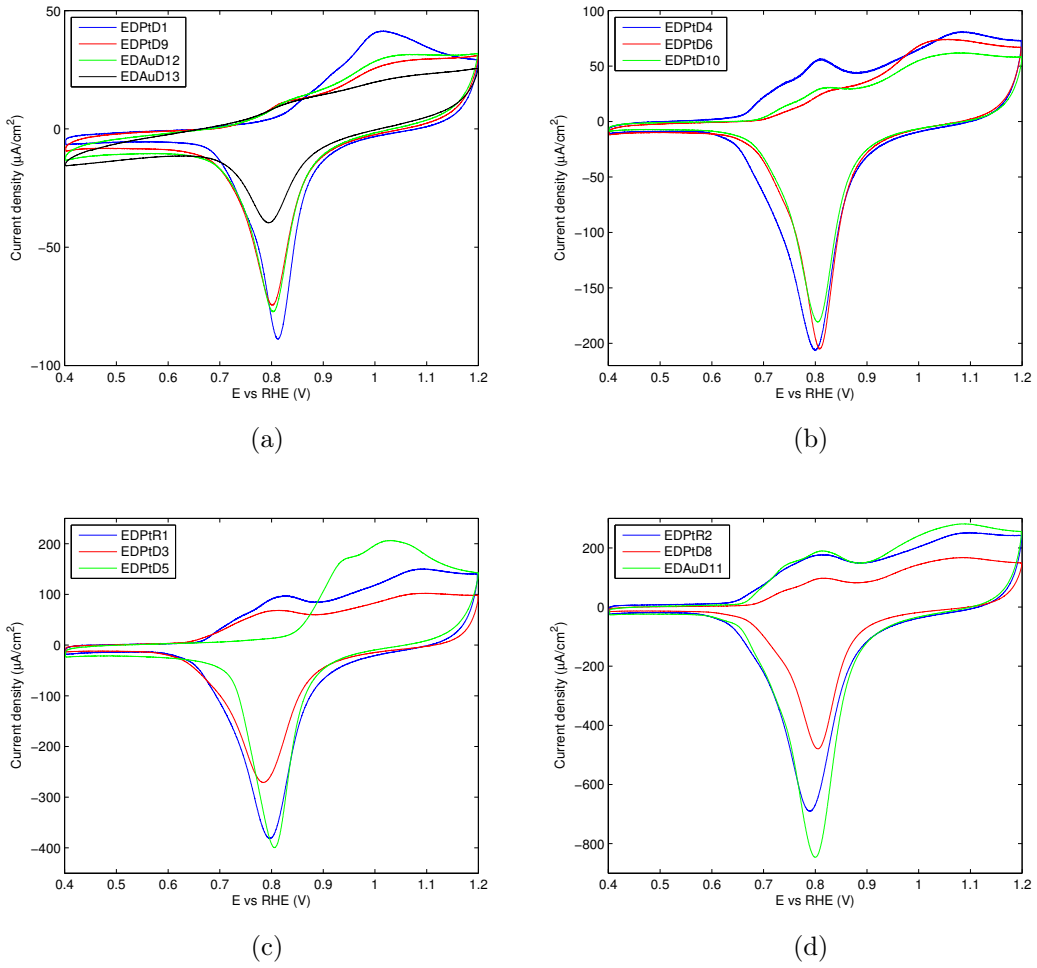

Figur 4.11: Voltammogram of palladium deposited electrodes in 0.1 M $HClO_4$. Seperated by current for clarity.

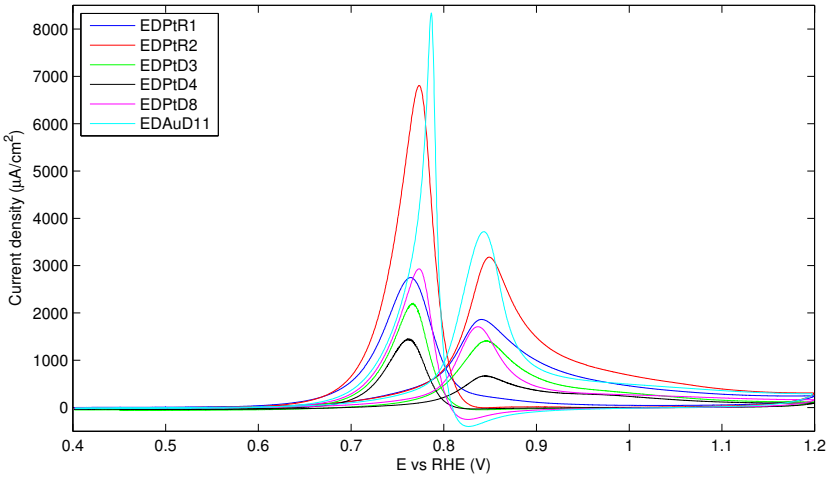

(a)

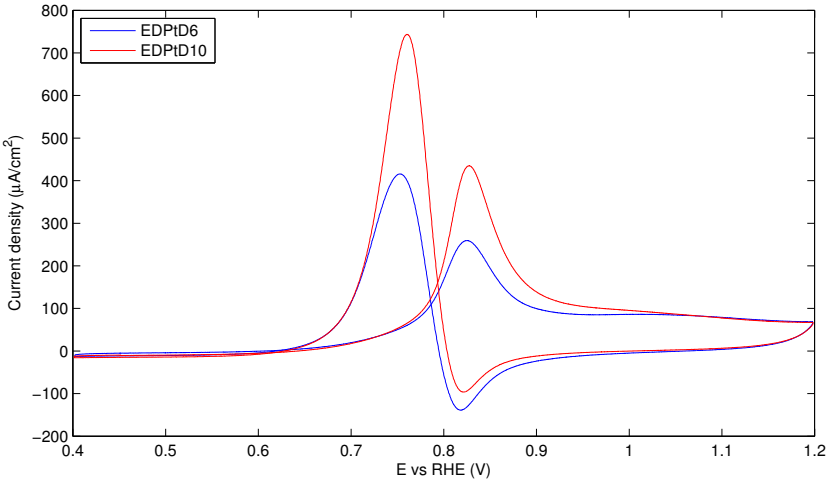

(b)

Figur 4.12: The figures show CVs for the electrodeposited palladium electrodes in 0.1 M $HClO_4$ and 1 M methanol (0.6 M for EDPtD6). Sweep rate 10 mV/s. Rotation at 1000 RPM for EDPtD3 and EDPtD4. Split in high and medium activity for clarity.

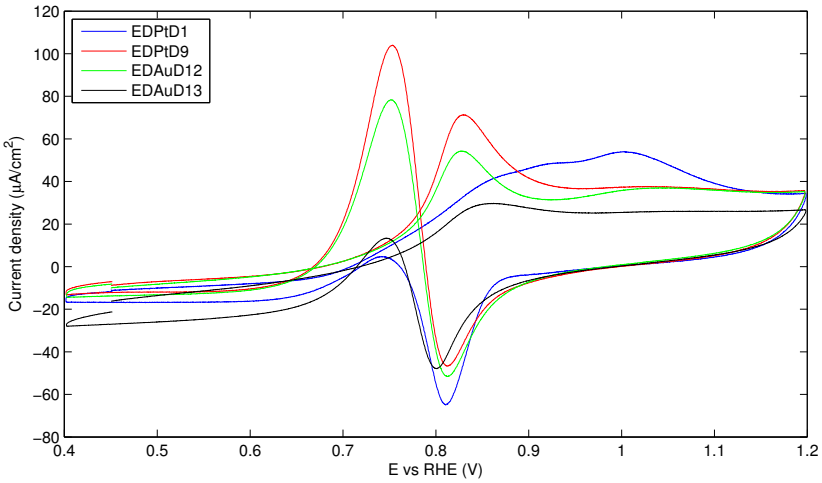

Figur 4.13: The figure show CVs for the electrodeposited palladium electrodes in 0.1 M $HClO_4$ and 1 M methanol for electrodes with low activity. Sweep rate 10 mV/s.

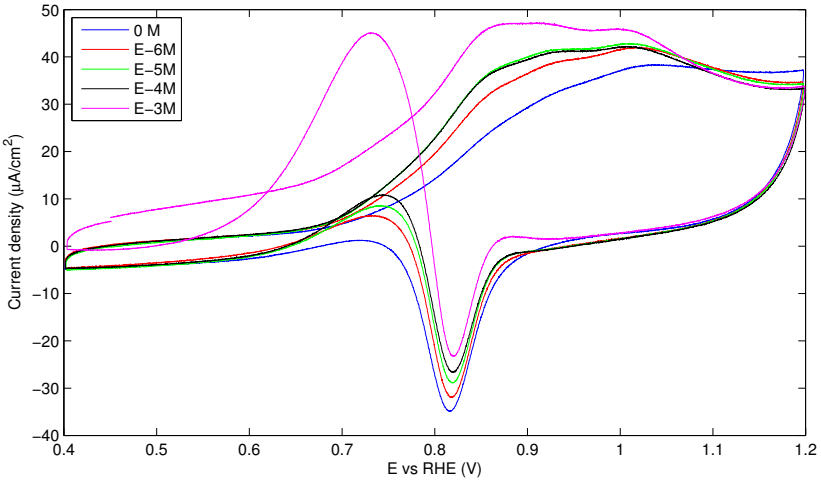

Figur 4.14: The figure show CVs on EDPtD1 in different concentrations of formic acid and 0.1 M $HClO_4$ and 1 M methanol. Sweep rate 10 mV/s.

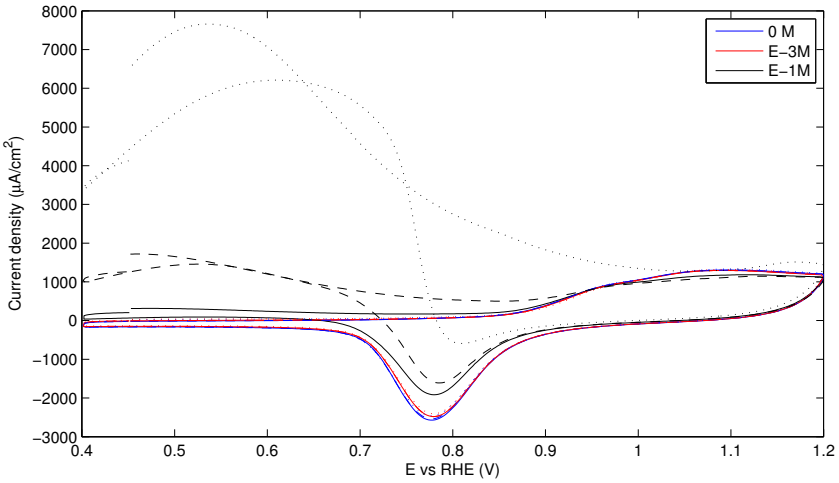

Figur 4.15: The figure show CVs on EDPtD5 in different concentrations of formic acid and 0.1 M $HClO_4$ and 1 M methanol. Dotted lines (:) are sweep number 1, Striped lines (–) are sweep number 5 and solid lines (-) are sweep number 10. Sweep rate 100 mV/s.

4.5 Microcell

Figure 4.16 shows the activiation of the platinum catalyst on the gold foil. It was done in 0.1 M $HClO_4$ solution and shows the regular hydrogen adsorption peaks for platinum. The voltammogram is a distorted a bit.

Figure 4.17 shows the current-time plot for constant potential of 1 V in a 0.1 M $HClO_4$ and 1 M methanol solution. The current drops quickly from the initial current and continues to drop over time. The signal is also a bit irregular. During the experiment we saw bubbles forming on the electrode surface.

In figure 4.18 we see voltammograms in the solution after the constant potential. Figure (a) is at 200 mV/s and was recorded before the ones at 10 mV/s. We can see that the current is steadily dropping for each cycle, both at 200 mV/s and 10 mV/s (b). The current density is also very high.

We can calculate the theoretical concentration of formic acid and formaldehyde in this cell by using the formula:

$$C = \frac{Q \times \eta_i}{F \times n \times V} \tag{4.42}$$

where Q is the charge, η_i the current efficiency, $F = 96485C/\text{mol}$ is the faraday constant, n the number of electrons transfered for each reaction and $V = 700\mu\text{L}$ the volume. The charge can be calculated by integrating the current-time plot 4.17. This gives $Q = 0.263C$. Using the values from 4.1.4 we can calculate the concentrations: $C_{\text{HCOOH}} = 2.92 \times 10^{-4}$ and $C_{\text{HCHO}} = 2.34 \times 10^{-4}$.

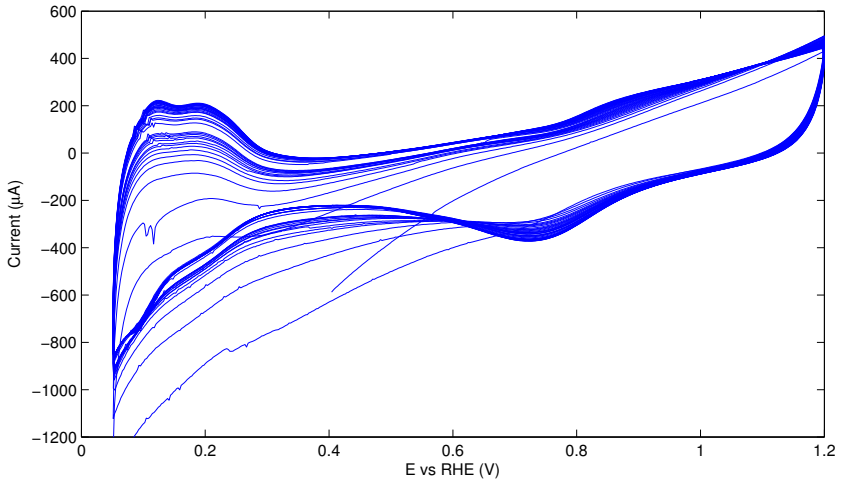

Figur 4.16: The figure shows CV for activiation of the platinum catalyst on gold foil. Several cycles at 100 mV/s in 0.1 M $HClO_4$

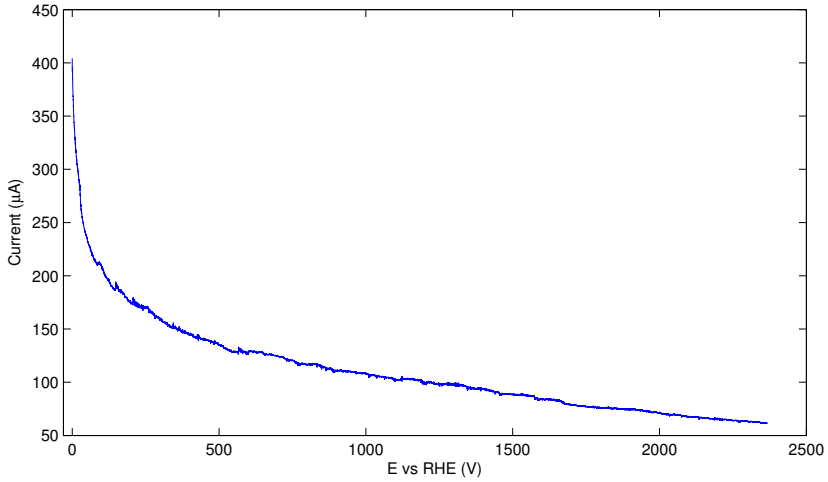

Figur 4.17: The figure shows current-time at the platinum catalyst electrode at 1 V constant potential for 40 minutes in 0.1 M $HClO_4$ and 1 M methanol.

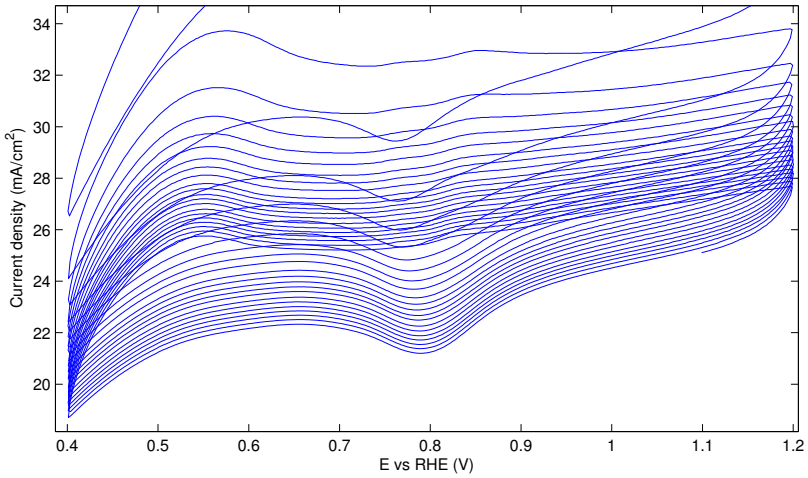

(a) 200 mV/s

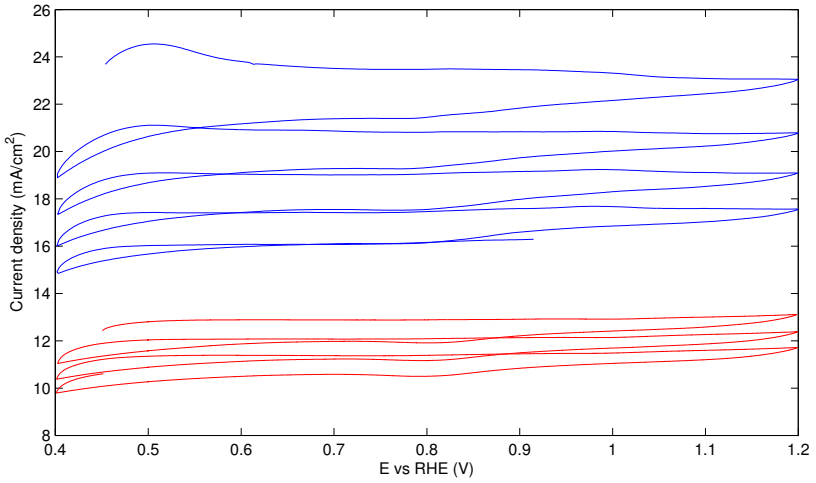

(b) 10 mV/s, some cycles not shown in between

Figur 4.18: The figures show CVs on the palladium wire electrode in 0.1 M $HClO_4$ and 1 M methanol (0.6 M for EDPtD6).

5. Discussion

5.1 Detection of species on gold

From figure 4.3 and 4.4 we see that we should be able to detect formic acid down to at least $10^{-}4$ M, even down to $10^{-}6$ M, but the large increase from 0 M to $10^{-}6$ M is unproportionally large compared to the increased current for higher concentrations. It possible that this large increase from 0 M to $10^{-}6$ M is due to adsorption of formate which can adsorp on gold [18]. We also see an increase in the cathodic reduction of the oxide layer which indicates more oxide formation. This can be an increase in the roughness because of the cycling [19], but not enough to compensate for the increase in anodic current. At 0.001 M and higher we see a very clear current for formic acid to diffentiate from the baseline in methanol.

For formaldehyde, we don't see a very clear difference before we have 0.01 M, although there is a significant difference between the baseline and 0.001 M (figure 4.4). For lower concentrations we have to compare the increased anodic current with the increase in the cathodic current. The increase in anodic current is only above the oxidation potential of gold and from this we can say that we probably can't detect formaldehyde at below 0.001 M concentration and that the increase in current is from the cycling.

We also have a set of these measurements for a platinum ring (figure 4.5) to see if it's viable, but as we can see, we can't differentiate the current for methanol oxidation and the increased current for formic acid oxidation until we have around 0.01 M, so this is not useful, and will not be used further.

From the modeling of the concentration (chapter 4.1.4) we see that the concentration

for formic acid, $C^{\text{ring}}_{HCOOH} = 3.56 \times 10^{-4} M$, should be able to be detected, but the concentration for formaldehyde is too low, $C^{\text{ring}}_{HCHO} = 2.56 \times 10^{-4} M$.

When we consider the actual experiments where these values are being used (figure 4.1 and 4.2) we fint a slight increase that might correspond to formic acid or/and formaldehyde. We see that the current at the platinum disk is much lower than for our theoretical example. Using a current of 0.2 $\text{mA}\,\text{cm}^{-2}$, we get the following concentration for formic acid: $C^{\text{ring}}_{HCOOH} = 7.74 \times 10^{-6} M$. This might be detectable, but it is a very low concentration. We can also see from the figure that there are some slight shifts at low potentials and the cathodic peak as well. Not high enough current that we can conclude with anything.

For the experiment with platinum catalyst on the disk we have a much higher current. At the time for the first voltammogram, we have a current of ca 5.5 $\text{mA}\,\text{cm}^{-2}$, which will give a concentration of well over 10^{-5} M. The problem here is that the voltammograms are clearly not stable enough to be of use. The voltammograms that corresponds to lower current on the disk have a higher current on the ring, in we also have a distortion on the voltammograms, probably from uncompensated resistance in the setup. We are unable to conclude anything from these voltammograms also because of the instability.

5.2 Palladium as the detector

5.2.1 Preliminary concentration measurements

Palladium has a high activity in formic acid at low potentials and low activity for methanol oxidation in acidic solutions [20, 21, 22]. This makes it ideal for detection of formic acid in a methanol experiment. Experiments on the palladium wire electrode (figure 4.6 shows a better distinction for low ($< 10^{-4}$ M) concentrations of formic acid than the gold electrode. We see an increase in current over almost the entire potential, and the oxide reduction peaks are not increased. This may have been masked by the formic acid oxidation which are cutting them short, but the slopes are almost identical.

Formaldehyde have also been tested (figure 4.7) and here we can see a significant difference from the baseline when formaldehyde is introduced to the system. We also

see that there are difficulties with seperating the voltammograms for concentrations up to $10^{-}3$ M. We can also see a significant distortion which again is probably from uncompensated resistance in the setup. From these results we can say that formaldehyde will be hard to detect at low concentrations on palladium. There is also the possibility that the resistance, or the reasons for it, are invalidating these results.

There is also the problem of having both formic acid and formaldehyde in the same solution, which will probably be the case for biproducts for methanol oxidation. Both of these reactions have their peaks at more or less the same potential. If one of the reactions will dominate over the other, we can only detect this specie. If they have approximately the same activity, we see that formic acid oxidation are active at lower potentials, and we could use this to determine the concentrations. From the results, formic acid will be much more active than formaldehyde, and it will be very hard to determine if there is formaldehyde in the solution.

5.2.2 Electrodeposition

For the electropdeposition process without rotation (figure 4.10a), we clearly different stages of electrodeposition for several of the samples. The initial steep drop corresponds to the ad-ion adsorption and nucleation of palladium, and the first plateu for the onset of palladium deposition. The second plateu corresponds to hydrogen reduction on the electrodeposited palladium [14]. These results are corroborated by figure 4.9 where we see a peak for the beginning of electrodepositon at 0.15 V, this is connected to the reduction of $[PdCl_4]^{2-}$, and a peak at 0 V which is connected to the hydrogen reduction on palladium [23]. At lower current densities for deposition (sample EDPtD6) we see that we do not have these seperate stages. This is probably because at such low current density, the first stage lasts the entire deposition.

When we apply rotation, we have very different E-t behaviour (figure 4.10b. The initial stage is still visible for some of the samples with a small drop in potential before it increases again. All potentials are also much higher than the samples of corresponding current density without rotation. This is because the rotation increases the transport of reactants to the surface, and less overpotential is needed to get the desired current density. At these potentials, we will not see any hydrogen reduction, and therefore the second stage is not possible.

The electrodeposition mechanism begins with $[PdCl_4]^{2-}$ which is adsorbed on the surface and reduced to Pd. A two-dimensional growth is preferred because the three-dimensional growth is inhibited by the adsorbed $[PdCl_4]^{2-}$ and Cl^- anions. After the first monolayer, island growth proceeds because of the hydrogen reduction and adsorbtion which displaces the $[PdCl_4]^{2-}$ ions [24, 14]. At low potentials we can also get Pd-hydride deposition.

5.2.3 Electrochemical characterization

We see that most of the voltammograms for the different palladium electrodeposited samples (figure 4.11 have the same basic shape with the onset of palladium oxide formation with peaks at about 0.7 V and 1.0 - 1.1 V, and a wide reduction peak at about 0.7 V. The samples EDPtD1 has a smaller current for det peak at 0.7 V and higher at 1 V while EDPtD5 has no peak at 0.7 V and and a higher current at 1.0 V. The oxide is palladium(II)oxide because of the low potential [12] It has been shown that the morphology of the palladium can influence the peaks [14], so we can assume that for the samples, except EDPtD1 and EDPtD5, we have the same basic morphology. Unfortunately, the samples were not looked at in a microscope, so we do not know the morphology.

Although they have the same basic morphology, we can clearly see that there must be a significant difference in the roughness and active surface area for these samples. We can use the reduction peak of the oxide as a basis for comparison. To get the most correct value we could integrate the oxide peaks and calculate the charge in each, but it is a good enough approximation to just use the peak current value to compare them. This has been done in table 4.1 and from this we can see that the active surface area roughly follows the Pd loading the samples, although EDPtD1 has a lower surface area and EDPtD8 has a higher surface area than expected. In the case of EDPtD8 we see that it was deposited with a high current density which may influence the surface area.

Most of the samples with rotation has the lowest activity, but these also had the lowest paladium loading, there are also samples with rotation among the ones with highest activity. So it seems that rotation does not have much influence on the surface. The color and evenness of the layer does not seem to influence the activity either, except as that it seems to be a concequence of the current efficiency.

Another consideration is the polishing of the electrodes for each new electrodeposition. This was done, but as we can see from figure 4.8 it was not done well enough. We can clearly see that at the Pt electrodes, we can still see a distinctive palladium voltammogram with oxide reduction peak at 0.7 V and the typical palladium hydrogen adsorption and absorption at low potentials [12]. We also see the increase in potential for this hydrogen behaviour for later samples, which means that there are more and more palladium in our platinum electrode. This has either not been polished good enough, or penetrated deeper into the electrode. This might be the reason that EDPtD1 behaves differently than the other samples. For the gold electrodes in figure (b) we see a small oxide reduction peak at 0.6 V and a small increase in hydrogen activity, but this is a much smaller than for platinum.

5.2.4 Methanol oxidation

The whole point of depositing palladium on these electrodes were to create an electrode that had the same properties as a pure palladium electrode in methanol, but as we can see from figures 4.12 and 4.13, almost all the samples show a significant activity in methanol. When we compare the voltammograms on these electrodes with the ones on palladium wire in formic acid (figure 4.6) we see that there might be a possibility to detect formic acid below 0.7 V in spite of the methanol oxidation, but it should be possible to create a palladium layer that is not active in methanol.

From the figures and table 4.1 we see that the methanol oxidation more or less follows our ranking for the surface area. This could be improved to get a better understanding of the methanol activity by dividing the methanl current by a pseudo surface area from the oxide reduction peak, but we will concentrate on the samples that looks promising. From the table we see that EDPtD5 is the sample with lowest activity in methanol with an almost identical voltammogram for only 0.1 M $HClO_4$ as for addition of 1 M methanol. EDPtD1 is the second best sample. Only these two were investigated further even though EDAuD13 was promising.

EDPtD5 has the highest amount of paladium loading and one of the highest activities in 0.1 M $HClO_4$, but the lowest for 1 M methanol. From figure 4.15 we see that we must have some sort of deactivation of the oxidation of methanol and formaldehyde. We see that for 0.1 M formic acid, it only takes four cycles before the activity is down to one fifth of the first cycle, and then another five cycles before it is almost down to the baseline again. The reason for this deactivation are not known, but it is

certainly the reason why the sample had so low activity for methanol.

The second promising sample was EDPtD1. We see from figure 4.14 that even though the results are not as good for the palladium wire, and we have some activity in methanol still, we can clearly see the activity for the formic acid compared to the baseline with 0 M formic acid, altough the voltammograms for 10^{-6} M to 10^{-4} M are very closely spaced. Attempts to reproduce these results were performed by using the paramaters for this sample on sample EDPtR1, EDPtR2, EDPtD3 and EDAuD11 but all these showed activity in methanol.

5.3 Methanol oxidation in small volume

We can see from figure 4.16 that we have a normal, if somewhat distorted, voltammogram for activation of the platinum catalyst on carbon black. This shows that the platinum catalyst electrode in the microcell works. From the results we know that we had formation of bubbles on the work electrode during the constant potential experiment designed to produce the biproducts. This is most likely the cause of the instabilities in the current-time plot (figure 4.17). From the theory, we can assume that this gas is a mixture of CO and CO_2. From the calculation of the concentration in the microcell, we should have been able to detect formic acid on the palladium wire electrode, but as we can see from figure 4.18 we had a response of very high current at both forward and backwards sweep with decreasing current for each sweep. This current might be because of CO-oxidation, which is active at these potentials on palladium [25, 26]. The high current, which is several times higher than formic acid oxidation in 0.1 M, makes this seem improbable, but the CO will in any case influence the current on the palladium wire.

6. Conclusion and further work

We have tried to develop a method to detect the indermediary species of methanol oxidation, formaldehyde and formic acid. To do this, we have developed a model for concentration at the ring in a rotating ring-disk electrode setup, but the results from experiments on a gold ring was not very successful. From the results in concentration of formic acid and formaldehyde on palladium wire electrode, we can conclude that palladium should be able to detect at formic acid down to a concentration of $10^{-}6$ M, and formaldehyde down to a concentratio of 0.001 M, maybe even lower.

Palladium was elecrodeposited in platinum and gold electrode in an attempt to create a palladium ring-electrode. We had one successful sample, but this could not be reproduced, and the other samples showed activity in methanol, or no activity at all. A microcell was used to detect byproducts by the previous palladium wire electrode. This experiment gave a high current from a different source, maybe CO-oxidation from dissolves CO, that would have masked any formic acid or formaldehyde oxidation.

As a suggestion for further work, we should try again to make a palladium ring electrode because of its sensitivity to formic acid oxidation. The microcell could be improved by building a custom cell for this where the gas can be removed before detection with a palladium electrode. Some of the experiments could also be repeated to get better cleaner values.

Bibliografi

[1] U.s. energy information administration, annual energy review 2011, tables 1.3, 2.1b-2.1f , 10.3, and 10.4.

[2] J. M. Ogden. Prospects for building a hydrogen energy infrastructure. *Annual Review of Energy and the Environment*, 24:227–279, 1999. Cited By :220 Export Date: 15 December 2014.

[3] Piotr Ochal. *Carbon-supported Ru @ Pt Core-shell Catalyst for Low Temperature Fuel Cells*. Thesis, 2012. Doktoravhandlinger ved NTNU.

[4] Wolf Vielstich Carl. H. Hamann, Andrew Hamnett. *Electrochemistry*. Wiley-VCH, second, completely revised and updated edition edition, 2007.

[5] T. Iwasita. *Methanol and CO electrooxidation*, volume 2, book section 41, pages 603–623. Wiley-VCH, 1 edition, 2003.

[6] E. Christoffersen, P. Liu, A. Ruban, H. L. Skriver, and J. K. Nørskov. Anode materials for low-temperature fuel cells: A density functional theory study. *Journal of Catalysis*, 199(1):123–131, 2001.

[7] E. Antolini. The problem of ru dissolution from pt-ru catalysts during fuel cell operation: Analysis and solutions. *Journal of Solid State Electrochemistry*, 15(3):455–472, 2011. Cited By :25 Export Date: 15 December 2014.

[8] Piotr Ochal, Jose Luis Gomez de la Fuente, Mikhail Tsypkin, Frode Seland, Svein Sunde, Navaneethan Muthuswamy, Magnus Rønning, De Chen, Sergio Garcia, Selim Alayoglu, and Bryan Eichhorn. Co stripping as an electrochemical tool for characterization of ru@pt core-shell catalysts. *Journal of Electroanalytical Chemistry*, 655(2):140–146, 2011.

[9] D. Bokach, J. L. G. De La Fuente, M. Tsypkin, P. Ochal, I. C. Endsjø, R. Tunold, S. Sunde, and F. Seland. High-temperature electrochemical characterization of ru core pt shell fuel cell catalyst. *Fuel Cells*, 11(6):735–744, 2011. Cited By :6 Export Date: 14 December 2014.

[10] Y. Garsany, O. A. Baturina, K. E. Swider-Lyons, and S. S. Kocha. Experimental methods for quantifying the activity of platinum electrocatalysts for the oxygen reduction reaction. *Analytical Chemistry*, 82(15):6321–6328, 2010. Cited By :113 Export Date: 15 December 2014.

[11] M. Łukaszewskil, M. Grdenl, and A. Czerwinski. Comparative study on hydrogen electrosorption in palladium and palladium-noble metal alloys. *J. New Mater. Electrochem. Sys*, 9(4):409–417, 2006.

[12] Michal Grdeń, Mariusz Łukaszewski, Gregory Jerkiewicz, and Andrzej Czerwiński. Electrochemical behaviour of palladium electrode: oxidation, electrodissolution and ionic adsorption. *Electrochimica Acta*, 53(26):7583–7598, 2008.

[13] Chi-Chang Hu and Ten-Chin Wen. Voltammetric investigation of palladium oxides iii: Effects of hydration and ph on the electrocatalytic properties of pd (iv) pd (ii) and the reduction behaviour of palladous oxide. *Electrochimica acta*, 41(9):1505–1514, 1996.

[14] F. Sarto, E. Castagna, M. De Francesco, T. M. Dikonimos, L. Giorgi, S. Lecci, M. Sansovini, and V. Violante. Morphology and electrochemical properties of pd-based catalysts deposited by different thin-film techniques. *International Journal of Hydrogen Energy*, 39(27):14701–14711, 2014.

[15] Allen J. Bard and Larry R. Faulkner. *Electrochemical methods: fundamentals and applications*, volume 2. Wiley New York, 1980.

[16] K. I. Ota, Y. Nakagawa, and M. Takahashi. Reaction products of anodic oxidation of methanol in sulfuric acid solution. *Journal of Electroanalytical Chemistry*, 179(1-2):179–186, 1984. Cited By :85 Export Date: 11 February 2015.

[17] Carl L. Yaws. *Yaws' Transport Properties of Chemicals and Hydrocarbons (Electronic Edition)*. Knovel, 2010.

[18] Angel Cuesta, Gema Cabello, Fabian W. Hartl, María Escudero-Escribano, Cristina Vaz-Domínguez, Ludwig A. Kibler, Masatoshi Osawa, and Claudio Gutiérrez. Electrooxidation of formic acid on gold: An atr-seiras study of the role of adsorbed formate. *Catalysis Today*, 202(0):79–86, 2013.

[19] Michael E. G. Lyons Laurence D. Burke. *Electrochemistry of Hydrous Oxide Films*, volume 18. 1986.

[20] Andrew Capon and Roger Parsons. The oxidation of formic acid on noble metal electrodes: Ii. a comparison of the behaviour of pure electrodes. *Journal of Electroanalytical Chemistry and Interfacial Electrochemistry*, 44(2):239–254, 1973.

[21] Margaretta M. Dimos and G. J. Blanchard. Evaluating the role of pt and pd catalyst morphology on electrocatalytic methanol and ethanol oxidation. *The Journal of Physical Chemistry C*, 114(13):6019–6026, 2010.

[22] Xiaoguang Wang, Weimin Wang, Zhen Qi, Changchun Zhao, Hong Ji, and Zhonghua Zhang. High catalytic activity of ultrafine nanoporous palladium for electro-oxidation of methanol, ethanol, and formic acid. *Electrochemistry Communications*, 11(10):1896–1899, 2009.

[23] K. Mech, P. Żabiński, R. Kowalik, and K. Fitzner. Kinetics and mechanism of [pdclx (h2o) 4- x] 2- x (x= 3, 4) complexes electro-reduction. *Journal of The Electrochemical Society*, 160(10):H770–H774, 2013.

[24] Hideo Naohara, Shen Ye, and Kohei Uosaki. Electrochemical deposition of palladium on an au(111) electrode: effects of adsorbed hydrogen for a growth mode. *Colloids and Surfaces A: Physicochemical and Engineering Aspects*, 154(1–2):201–208, 1999.

[25] Lam Wing H. Leung and Michael J. Weaver. Extending surface-enhanced raman spectroscopy to transition-metal surfaces: carbon monoxide adsorption and electrooxidation on platinum-and palladium-coated gold electrodes. *Journal of the American Chemical Society*, 109(17):5113–5119, 1987.

[26] Andrzej Czerwiński. The adsorption of carbon oxides on a palladium electrode from acidic solution. *Journal of Electroanalytical Chemistry*, 379(1):487–493, 1994.